Carbon 149 (2019) 419–435

Contents lists available at ScienceDirect

Carbon

journal homepage: www.elsevier.com/locate/carbon

Why some carbons may or may not graphitize? The point of view of thermodynamics

Philippe Ouzilleau [a,*], Aïmen E. Gheribi [a], Patrice Chartrand [a], Gervais Soucy [b], Marc Monthioux [c]

[a] Centre de Recherche en Calcul Thermochimique (CRCT), Polytechnique Montréal, Département de génie chimique, Montréal, Québec, H3C 3A7, Canada
[b] Département de génie chimique et de génie biotechnologique, Université de Sherbrooke, Sherbrooke, Québec, J1K 2R1, Canada
[c] Centre d'Élaboration des Matériaux et d'Études Structurales (CEMES), UPR-8011 CNRS, Université de Toulouse, BP 94347, F-31055, Toulouse Cedex 4, France

ARTICLE INFO

Article history:
Received 13 November 2018
Received in revised form
27 March 2019
Accepted 6 April 2019
Available online 12 April 2019

ABSTRACT

Not all carbons graphitize in equal measure. Some will develop a structure which approaches the one of perfect graphite (graphitizable carbons) upon heat treatment, while others will not (non-graphitizable carbons). The present work develops a phenomenological model for the conceptual understanding of graphitizability (capacity to graphitize). To support this model, a mathematical formalism, inspired from thermodynamics, is proposed to calculate the Ultimate Graphitizability (η_g) of some graphitizable and non-graphitizable carbon materials. η_g is the average interlayer spacing (d_{002}) of a graphenic carbon following graphitization at $\sim$ 3400 K. η_g can be estimated assuming a topological graphitization mechanism operating between 1700 K and 3400 K. Two independent variables define η_g: $d_{002}(T_\alpha)$ and $d_{002}(T_\beta)$. T_α and T_β are arbitrarily selected temperatures between 1700 K and 2550 K (the graphitization threshold). In order to better understand the parameters affecting $d_{002}(T_\alpha)$ and $d_{002}(T_\beta)$, new carbonization/graphitization experimental results are presented. These suggest that $d_{002}(T_\alpha)$ and $d_{002}(T_\beta)$ are correlated to the oxygen/hydrogen composition ratio and the relative mesoscale crystallite orientation of some graphitizable carbons following the end of primary carbonization.

© 2019 The Authors. Published by Elsevier Ltd. This is an open access article under the CC BY-NC-ND license (http://creativecommons.org/licenses/by-nc-nd/4.0/).

1. Introduction

Franklin [1,2] is often credited [3] as the author of the first conceptual model for the thermal graphitization process. Thermal graphitization is generally defined as the development of graphitic order from initially non-graphitic carbons through high temperature heat treatment. While Franklin's model undeniably provided a good premise to understand some of the fundamentals of the graphitization process, other models were subsequently proposed [4–8]. One key model was presented by Oberlin et al. [5,9–14]. Essentially, this model suggested that the graphitization of carbons proceeded through the progressive ordering, with increasing heat treatment temperature (T_{HT}), of carbon atom clusters named LMOs (Local Molecular Orientation clusters). LMOs are ensembles of mutually well-oriented graphenic crystallites (the conceptualisation of these crystallite taking strong inspiration from Franklin's model). Oberlin's model key contribution was to highlight that the average size of the LMOs, which is correlated to the heteroatoms (e.g. oxygen) over hydrogen atoms ratio following heat treatment of a precursor carbon at approximately 673 - 873 K, is a key factor to graphitizability. Graphitizability is defined as the ability of carbons to develop graphitic structure following graphitization heat treatment. Carbons with low ratios develop larger LMOs and thus possess a higher graphitizability than carbons with high ratios. Carbons with low graphitizability are classified as non-graphitizable carbons while high graphitizability carbons are classified as graphitizable carbons. According to Oberlin's approach, all carbons, regardless of graphitizability, are composed of said LMOs. Differences in the average LMO size explain the variable graphitizability of one carbon relative to another. The graphitizability of a carbon is thus primarily defined by the average LMO size of the material. This approach has been criticized by Harris [3] on the basis that it did not clearly explain how the size of the LMOs could be related to the non-graphitizability of some carbons. Harris [3] proposed that non-graphitizable carbons are instead composed of

* Corresponding author.
E-mail address: philippe.ouzilleau@polymtl.ca (P. Ouzilleau).

https://doi.org/10.1016/j.carbon.2019.04.018
0008-6223/© 2019 The Authors. Published by Elsevier Ltd. This is an open access article under the CC BY-NC-ND license (http://creativecommons.org/licenses/by-nc-nd/4.0/).

fullerene-related structures. It was suggested that the presence of strong curvatures [3,6,15] in such structures could explain the non-graphitizability of non-graphitizable carbons. Both perspectives on non-graphitizable carbons are not mutually exclusive (this will be further discussed over the course of the present paper). Important to note, it was previously demonstrated [11,16–18] that graphitizability is a continuous property. Specifically, graphitizability is distributed on a connected spectrum ranging from non-graphitizable carbons, to semi-graphitizable [19] carbons and, finally, to graphitizable carbons. This may suggest that the transformation behaviour of both graphitizable and non-graphitizable carbons during graphitization heat treatment share a common structural origin. Thus, it would be critical for any graphitizability model to quantitatively demonstrate its ability to describe graphitizability as a spectrum.

Considering the importance of graphitization, graphitizable carbons and non-graphitizable carbons for future applications of carbon materials (heat shields for space exploration [20], performance enhancers for Li-ion batteries [21], development of activated carbons [22] for atmospheric CO_2 capture), the present work aims to propose a new thermodynamic model to quantitatively predict the graphitizability of some graphitizable and non-graphitizable carbons following graphitization heat treatment. The proposed approach of the paper is inspired from previous work [7,19,23] by Ouzilleau et al. While previous quantitative graphitization modelling has primarily focused on kinetic approaches [4], Ouzilleau showed that thermodynamics could provide a valuable complementary understanding of some critical aspects of the general process (e.g. the so-called graphitization temperature threshold [19]). The thermodynamic background of the present graphitizability model is a logical continuation of the scientific discussions previously initiated by Ouzilleau [7,19,23].

For the sake of clarity, the terminology of the paper, inspired from the recommendations of Fitzer et al. [24], is presented here.

- Graphitic carbon: all allotropic configurations of carbon in the form of graphite regardless of the presence of structural defects. Long-range order three-dimensional stacking is significantly detectable in graphitic carbons.
- Non-graphitic carbon: all solids of the element carbon consisting of two-dimensional graphenic structures, but without any measurable crystallographic long-range order in the c-direction (with the exception that graphenic layers exhibit some parallel stacking). A non-graphitic carbon is a turbostratic carbon [19].
- Graphitization: solid-state transformation of non-graphitic carbon to graphitic carbon by means of high temperature heat treatment.
- Graphitization heat treatment: solid-state transformation process of non-graphitic carbon by means of high temperature heat treatment in order to achieve graphitic ordering regardless of the extent of said resultant ordering.

The paper is organized as follows. Section 2 will propose a simplified graphitization mechanism for the graphitization heat treatment process. This mechanism will serve as a basis to model graphitizability. The structural model at the forefront of this new mechanism, which is inspired from what was previously proposed by Ouzilleau [7], will be presented. It will be shown that the graphitization mechanism can be modelled with a first-order non-homogeneous differential equation in order to produce quantitative calculations for the effect of T (considering $T = T_{HT}$) on one of the most significant graphitization properties [4]: the average interlayer spacing of the graphenic layers (d_{002}). Predictions of the model will be compared to experimental measurements obtained from various graphitizable and non-graphitizable carbons. Section 3 will present an experimental study on the carbonization/graphitization of some graphitizable carbons. The focus will be on how graphitizability could be related to some chemical and structural properties developed prior to graphitization; specifically, to properties measured following the end of the primary carbonization process [5,18,19]. Primary carbonization reaches its penultimate stage at approximately 673 - 873 K (the exact temperature of completion depending on the precursor composition and other factors) and produces a brittle solid material (semicoke) from an initial precursor carbon.

2. Proposing a topological graphitization mechanism to model graphitizability

2.1. Structural and thermodynamic assumptions

Proposing a structural model for non-graphitizable carbons is a complex endeavour. There exists a lack of knowledge on what truly constitutes a non-graphitizable carbon [3]. The evidence for this lies in the number of past models developed for these materials, some providing a general overview while others focus on describing a particular stage of development of the material following heat treatment. For example, models for non-graphitizable carbons include the Franklin's model [1], the model [25] of Ban, Crawford and Marsh, the model of Harris [3] and the LMO model of Oberlin [17] (the latter being one of the few models applicable to both graphitizable and non-graphitizable carbons). Models for non-graphitizable carbons based on the persistent presence at high temperature of sp^3 -bonded carbon atoms were rejected [3] by Harris on the basis that sp^3 carbon atoms would be highly unstable at temperatures [7] typical of the graphitization process ($T > 1700$ K). For example, Diaz [26] reported that the concentration of sp^3 -bonded carbon atoms in a non-graphitizable carbon film gradually diminished to zero at $T = 1300$ K. Moreover, the difficulty of developing a structural model for non-graphitizable carbons is further compounded if such a model aims at simultaneously producing quantitative predictions for the graphitizability spectrum of carbons (graphitizable, semi-graphitizable, non-graphitizable). As stated in Section 1, this specific modelling criteria is critical in order to produce physically significant calculations regarding graphitizability. Thus, some simplifying structural and thermodynamic assumptions are required. Most of these were detailed elsewhere [7,19,23] and will be summarily restated in Sections 2.1, 2.2 and 2.3 for the sake of conceptual clarity.

In the present model, a cluster approach is proposed for the structure of graphitizable and non-graphitizable carbons. In this approach, carbon atoms are assumed to be distributed in two types of clusters: the mGBs (mesoscale Grain Boundary) and the LMOs (Local Molecular Orientation). A cluster is defined as a region of space which encompasses a group of carbon atoms whose internal collective structure is not required to be uniform. As stated in Section 1, LMOs are ensembles of mutually well-oriented graphenic crystallites. The structure of mGBs, on the other hand, is less organized. It is assumed [7,16] that carbon atoms in mGBs are turbostratic (turbostratic meaning [7,27] two-dimensional crystallographic order) and non-graphitizable. The non-graphitizable character of carbon atoms in mGBs could be explained by the presence of strong curvatures [6,15] in the graphenic structure of said mGBs. This could be due to the important presence of non-planar (high energy) defects [7,16] (such as the heptagonal defect [28]). It is assumed that the important concentration of these high energy defects "freezes" the defective structure of mGBs (assuming a high activation energy for the thermal annealing of such high distortion defects). Frozen carbon atoms are thus non-graphitizable

by normal heat treatment.

As stated previously, LMOs are defined as ensembles of mutually well-oriented graphenic crystallites. Carbon atoms in LMOs are distributed [7] in two quasi-phases: the IM (Intercrystalline Matter) and the CC (Coke Crystallites). In this work, a quasi-phase is defined, in the thermodynamic sense, as a region of space which encompasses a group of carbon atoms whose internal collective structure is somewhat uniform. Thus, both the CC and the IM exhibit a phase-like behaviour from the perspective of thermodynamics. The CC is composed of idealized graphenic crystallites which will be called henceforth coke crystallites [23]. The structure of the CC is relatively uniform as its constituting coke crystallites are all built from the same graphenic template. The IM includes the cross-linking intercrystalline molecules and the numerous intercrystalline voids located between the individual coke crystallites. The IM provides structural stability to the LMO. Locally, single intercrystalline molecules may vary in shape and size. However, the volume occupied by said molecules over the total volume of the IM in a LMO is low enough so that this local variability is statistically negligible. Hence, the IM can be approximated as some kind of highly diffused quasi-uniform medium (a quasi-phase). The size (i.e. diameter) of a LMO is defined with the variable L^{LMO} (Fig. 1a). Finally, the finite idealized structure of coke crystallites in LMOs is characterized by three structural parameters: the coke crystallite diameter (L_a), the coke crystallite height (L_c) and the average interlayer spacing (d_{002}). Fig. 1 presents one possible configuration of mGBs and LMOs around a closed pore in a given carbon material. The diameter of a closed pore is defined by D_{pore} in Fig. 1a. In the case of graphitizable carbons, Oberlin model intrinsically showed that D_{pore} would be greater than in the case of non-graphitizable carbons (as L^{LMO} is larger [9] in graphitizable carbons than in non-graphitizable carbons). For a graphitizable carbon, the pore of Fig. 1 would be called a mesopore [7]. For non-graphitizable carbons, the closed pore of Fig. 1 would be called a micropore (because of the inherent small value of D_{pore}). Critical to note, this simplified representation of the porous structure of graphitizable and non-graphitizable carbons is limited compared to other thermodynamic models for porous carbons such as the model of Botan et al. [29]. The present D_{pore} descriptor should thus only be considered as a simple, qualitative criteria which may help differentiate non-graphitizable from graphitizable carbons.

One of the key thermodynamic parameters of the present paper is the critical temperature T_c. This parameter was previously defined [19] in order to model graphitization with a thermodynamic formalism similar to the one of second-order transitions. However, it must be stated that graphitization is not a thermodynamic transition per se. It is more suitable to describe graphitization as an irreversible transformation which progressively reorganizes the carbon nanostructure from one non-equilibrium state to another non-equilibrium state while approaching (as much as possible) the perfect graphite equilibrium state. Although classical thermodynamics models [30] are typically developed for reversible equilibrium processes, it is also possible to elaborate thermodynamic formalisms, under restrictions, for some irreversible non-equilibrium processes. For example, one fundamental condition [31] to be respected for such non-equilibrium developments is the *local equilibrium hypothesis*. Practical examples of irreversible thermodynamic models exist in the literature [32–34].

2.2. Phenomenological description of the topological graphitization mechanism

The present view on graphitization heat treatment is built on the general principles of the previous SOST (Second-Order Structural Transformation) model [19], with additional elements taken from the previously proposed representation [7] of topological defects in graphitizable carbons. Topological defects [7] are defined as intralayer imperfections located in the inner structure of the graphenic planes of merged coke crystallites. The key principle of the approach is that only the LMOs possess the capacity to graphitize through the ordering of the CC by the progressive densification of the IM (which is itself too diffuse to graphitize on its own). mGBs are highly defective clusters which do not possess any inherent graphitic order. As for the IM, in its initial state, it is not graphitic per se. It would be better described as a gas-like medium, a feature first exploited by Franklin [1] to measure the proportion of IM in heat treated carbons as a function of L_a. Only when the IM is progressively incorporated to the CC can graphitic order (potentially) develop in the overall LMO. The final extent of the graphitic order (or lack of graphitic order)is dependent on various factors, one being the average extent of the LMOs (L^{LMO}). Concerning the effect of graphitization heat treatment on LMOs, it is supposed that the irreversible transformation is in fact a sequence of two interlinked processes separated by a critical temperature threshold (T_c). Fig. 3 presents the proposed phenomenological graphitization mechanism for graphitization heat treatment assuming that the process starts at some temperature T_i^0 and reaches an end state (i.e.

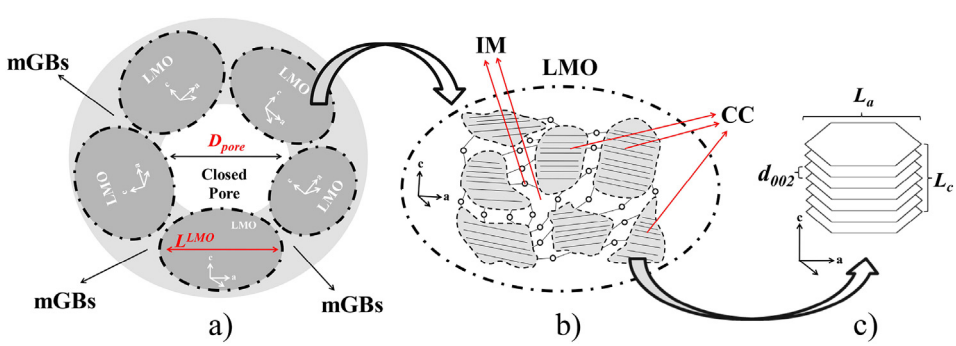

Fig. 1. The proposed cluster approach [7] for the organization of carbon atoms in graphitizable, semi-graphitizable [19] and non-graphitizable carbons following the end of primary carbonization [18]: (a) Simplified representation of a possible arrangement of Local Molecular Orientation clusters (LMOs) and mesoscale grain boundaries (mGBs) around a closed pore (micropore in the case of non-graphitizable carbons [3], mesopore in the case of graphitizable carbons [7]). L^{LMO} is the average size of a LMO. D_{pore} is the average size of a pore; (b) Structure of a LMO consisting of the Coke Crystallites quasi-phase (CC), which includes all individual independent coke crystallites [23] (light grey), and of the Intercrystalline Matter quasi-phase (IM), which includes all intercrystalline molecules (white circles) and the intra-LMO voids between the coke crystallites; (c) Idealized structure [23] of a coke crystallite. L_a is the average coke crystallite diameter. L_c is the average coke crystallite height. d_{002} is the average interlayer spacing of the graphenic layers. The cluster approach is limited [7] to carbons which reached the semicoke stage (i.e. completion of the primary carbonization process [18]). (A colour version of this figure can be viewed online.)

graphitizability limit) at some temperature T_e^0. Ouzilleau calculated [7,19] $T_i^0 \sim 1700$ K and $T_c \sim 2550$ K based on thermodynamic calculations for the graphitization process. Details in Fig. 3 are as follows (remembering that $T_{HT} = T$):

- If $T_i^0 \leq T < T_c$: this is the *merging and flattening* process. In this process (Fig. 3b), independent coke crystallites in LMOs progressively merge up to T_c. The density difference between the IM and the CC progressively decreases. The merging process may be imperfect and generate *annealable topological defects* (ATD) between mutually dependent merged crystallites (ATD are represented with green rectangles in Fig. 3b). An example of such an ATD [7] could be the Dienes defect (the recommended designation for the double pentagon/heptagon pair according to Monthioux and Charlier [35], previously called Stone-Wales defect) or the single vacancy defect [36,37]. Other types of topological defects such as the Thrower defect [35] (a single pentagon/heptagon pair), the Stone-Wales defect [35] (a double hexagon/pentagon pair), the 555–777 defect [38] (a grouping of three pentagonal defects and three heptagonal defects), the single pentagonal defect [28], the single heptagonal defect [28], the multiple vacancy defect [36,37] and the line defect [37,39] are assumed to be too energetic to be considered ATDs. Fig. 2 presents the structure of the Dienes defect. The progressive annealing of ATDs flattens the graphenic layers of the LMO. No structural change occurs in mGBs as the defects in such structures are not able to heal with heat treatment. At the frontier between neighbouring LMOs (the mGBs i.e. the dash-dotted line in Fig. 1a and b and 3), some *non-annealable defects* (NADs) are generated by the merging of the peripheral coke crystallites of said LMOs. It is proposed that these NADs are non-annealable due to the high distortion level of their topological structure, similar to carbon atoms in mGBs (the mGBs quasi-phase being itself composed of ensembles of NADs). Indeed, geometric constraints drastically increase (relative to ATDs) the activation energy for the onset of thermal annealing in all NADs.
- If $T = T_c$: coke crystallites in LMOs have fully merged (Fig. 3c). The density difference between the IM and the CC is null. If all ATDs are annealed when the material reaches T_c, the graphenic layers are perfectly flat. If some lingering ATDs (green rectangles in Fig. 3c) remain in the LMOs at T_c, some degree of distortion remains in the graphenic layers. Concerning mGBs, no significant structural change occurs. Concerning NADs, the maximal concentration (per mole of carbon) of these non-graphitizable defects is reached in the material at T_c. This concentration is inversely proportional to the size of the LMOs (i.e. carbon with larger LMOs have smaller NADs concentrations per mole of carbon atoms compared to those with smaller LMOs).
- If $T_c < T \leq T_e^0$: this is the *residual healing* process (Fig. 3d). In this process, coke crystallites in LMOs have fully merged. Reorganization by graphitization heat treatment proceeds through the annealing of all lingering ATDs (green rectangles in Fig. 3c and d) originating from the critical threshold step (Fig. 3c). If no ATDs remained at T_c, no residual healing occurs in LMOs between T_c and T_e^0 (thus the transformation by graphitization heat treatment has reached its limit). The annealing of ATDs is the interlink between the merging and flattening process (Fig. 3b) and the residual healing process (Fig. 3d). The progress of the reorganisation by graphitization heat treatment (measured by the d_{002} value following heat treatment) reaches a limiting value at T_e^0. At this stage, graphenic layers in LMOs are perfectly flat, but perfect graphitic order ($d_{002} = 0.3354$ nm) is not necessarily reached. The graphitizability limit of the LMO is a consequence of the number of ATDs generated by its merging and flattening process (as the graphitization mechanism is fuelled by the local annealing of ATDs [4]). Moreover, the lower the value of L^{LMO}, the lower the maximal (potential) amount of ATDs which can be produced by merging and flattening. Thus, a carbon with a high L^{LMO} value will tend to graphitize well under normal circumstances as it will have a high probability of developing numerous ATDs. Important to note, a low average L^{LMO} value is also associated to a high number of total NADs in the mesostructure. For this reason, a high number of NADs is implicitly correlated to low graphitizability. Hence, two important criteria to reach perfect graphitic order are to have an infinite average value for L^{LMO} (Fig. 1a) and to have a graphitization process operating at temperatures greater than T_c (i.e. the temperature threshold for the establishment of true graphitic ordering [7,19]).

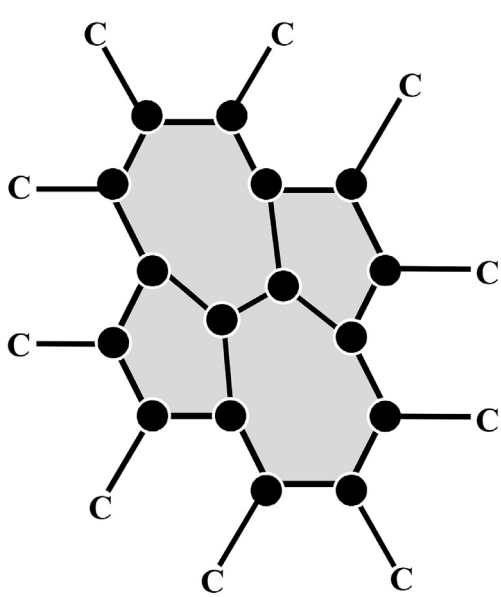

Fig. 2. The Dienes defect [40] (the recommended designation for the previously called Stone-Wales defect, according to Monthioux and Charlier [35]). Black circles represent carbon atoms shared by three neighbouring sites.

2.3. Mathematical approach to the topological graphitization mechanism

The basis of the present graphitizability model is the separation of the carbon population into two quasi-phases: the mGBs and the LMOs. To model graphitizability, the model requires a first *Ansatz* (a primitive mathematical hypothesis) for the d_{002} variation of any possible graphenic structures which could be located in mGBs following heat treatment between temperatures T_i^0 and T_e^0:

Ansatz 1 (Eq. (1)): "Relative to LMOs, mGbs will never graphitize in the sense that graphitization heat treatment will not significantly decrease the interlayer spacing of any graphenic structures in this specific cluster, if such graphenic structures are indeed present in mGBs."

$$d_{002,mGBs}\left(T_i^0\right) - d_{002,mGBs}\left(T_e^0\right) \ll d_{002,LMOs}\left(T_i^0\right) - d_{002,LMOs}\left(T_e^0\right) \quad (1)$$

In Eq. (1), $d_{002,mGBs}(T_i^0)$ and $d_{002,mGBs}(T_e^0)$ are the interlayer spacings of carbon atoms in mGBs respectively following heat treatment at T_i^0 and T_e^0. $d_{002,LMOs}(T_i^0)$ and $d_{002,LMOs}(T_e^0)$ are the

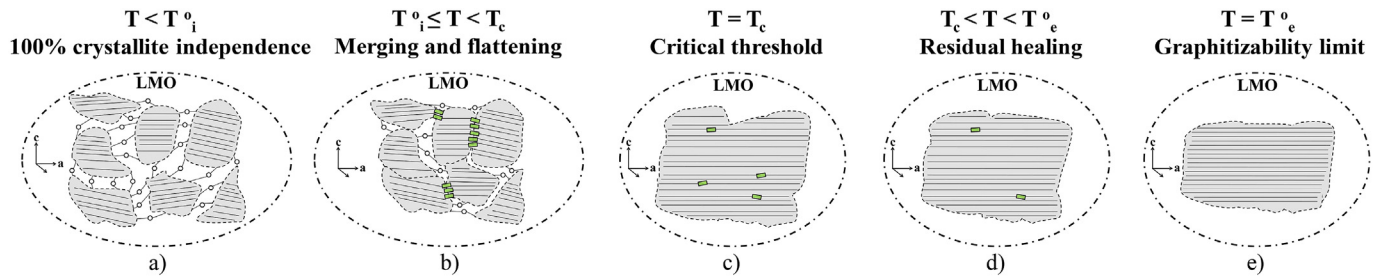

Fig. 3. The topological graphitization mechanism of carbon atoms in LMOs during graphitization heat treatment, inspired from the SOST model [19]: (a) Structure of the LMO prior to the onset of graphitization heat treatment; (b) The merging and flattening process where imperfect merging generates annealable topological defects (ATDs). ATDs are represented with green rectangles and could be viewed as two-dimensional Dienes [35,40,41] defects (or other types of low-deformation planar defects such as the single vacancy defect [36,37]); (c) Structure of the LMO at T_c where the densities of the IM and the CC are equal. Here, the merging and flattening process ($T_i^0 \leq T < T_c$) did not anneal all ATDs hence some lingering ATDs remain at T_c. Lingering ATDs are formed when ATDs not annealed by the merging and flattening process persist in LMOs up to T_c; (d) The residual healing process which progressively removes lingering ATDs formed at the critical threshold T_c; (e) The graphitizability limit which is implicitly correlated to the number of non-annealable defects (NADs) formed during the merging and flattening process ($T_i^0 \leq T < T_c$) at the LMO surface (dash-dotted line). The maximal concentration of NADs is reached at T_c. The maximal concentration of NADs is constant from T_c to T_e^0. Based on Ouzilleau's calculations[7,19], $T_i^0 \sim 1700$ K and $T_c \sim 2550$ K. (A colour version of this figure can be viewed online.)

interlayer spacings of carbon atoms in LMOs respectively following heat treatment at T_i^0 and T_e^0. *Ansatz* 1 is important because it simplifies the modelling of graphitizability, both for non-graphitizable and graphitizable carbons, solely on the behaviour of carbon atoms in LMOs during graphitization heat treatment. It is a reasonable assumption because mGBs rarely develop graphenic structures of sufficient size to even produce a graphitic signature in the first place. Based on this primary assumption, Eq. (2) is proposed as a logical consequence of Eq. (1):

$$d_{002}\left(T_i^0\right) - d_{002}\left(T_e^0\right) \sim f\left(d_{002,LMOs}\left(T_i^0\right) - d_{002,LMOs}\left(T_e^0\right)\right) \tag{2}$$

In Eq. (2), $d_{002}(T_i^0)$ and $d_{002}(T_e^0)$ are the interlayer spacings of the overall carbon material (mGBs + LMOs) respectively following heat treatment at T_i^0 and T_e^0. As stated, the claim of *Ansatz 1* is that the change in d_{002} of the overall carbon following graphitization heat treatment can be approximated as a function of solely the change of d_{002} in LMOs (hence Eq. (2)). The contribution of carbon atoms in mGBs to the measurement of the overall decrease of d_{002} is negligible. Thus, the present mathematical formalism for graphitizability can be applied to graphitizable and non-graphitizable carbons.

As described in Section 2.2, in LMOs, the merging and flattening process (Fig. 3b) and the residual healing process (Fig. 3d) are interlinked. The residual healing process anneal lingering ATDs which were generated, but not annealed, by the merging and flattening process. Thus, for a given graphitization heat treatment process ($T_i^0 < T < T_e^0$) where only T (remembering $T = T_{HT}$) is varied, both processes (merging and flattening and residual healing) should be described with the same general mathematical expression for their transformation order parameter. This expression is the previously defined Graphitization Order Parameter [7] (defined with Ω^0). Depending on the studied temperature range, the value of Ω^0 is calculated by Equations (3)–(6):

$$\Omega^0 = 1 \quad ; \text{ for } T < T_i^0 \tag{3}$$

$$\Omega^0 = 1 + \int_{T_i^0}^{T} \theta_c \left(\left|\frac{T}{T_c} - 1\right|^{\beta} - \gamma^{-1}\right) \mathrm{d}T \quad ; \text{ for } T_i^0 \leq T \leq T_c \tag{4}$$

$$\Omega^0 = 0 + \int_{T}^{T_c} \theta_c \left(\left|\frac{T}{T_c} - 1\right|^{\beta} - \gamma^{-1}\right) \mathrm{d}T \quad ; \text{ for } T_c \leq T \leq T_e^0 \tag{5}$$

$$\Omega^0 = 1 \quad ; \text{ for } T_e^0 < T \tag{6}$$

The physical interpretation of Ω^0 depends on the studied temperature range. If T lies between T_i^0 and T_c, Ω^0 describes the relative independence [7] of coke crystallites in LMOs (1 at T_i^0, 0 at T_c). Between T_c and T_e^0, Ω^0 describes the probability of not finding lingering ATDs, assuming said lingering ATDs were generated during merging and flattening. Ω^0 is equal to 1 at T_e^0 (all lingering ATDs present at T_c are removed). At T_c, this probability is 0 (again, assuming that lingering ATDs were generated).

Previous work [7,19] reported the theoretical values of the various critical parameters of Equations (4) and (5). The detailed development of these parameters will not be discussed here. T_i^0 and θ_c are respectively valued at 1715±35 K and $-3.83 \times 10^{-3} \pm 7.5 \times 10^{-5}$. T_c is equal to 2550±50 K. β and γ are respectively valued at −0.2 and 0.8. The only new parameter here is T_e^0. However, by referring to a temperature difference analogy with T_i^0 and T_c, T_e^0 can be evaluated based on the symmetry of Ω^0. This yields $T_e^0 =$ 3385±65 K. Similar to what was previously [7] presented, Ω^0 can be translated as a function of various threshold d_{002} values with Equations (7) and (8):

$$\Omega^0 = 1 + \frac{d_{002}(T) - d_{002}\left(T_i^0\right)}{d_{002}\left(T_i^0\right) - d_{002}(T_c)} \quad ; \text{ for } T_i^0 \leq T \leq T_c \tag{7}$$

$$\Omega^0 = 0 + \frac{d_{002}(T_c) - d_{002}(T)}{d_{002}(T_c) - d_{002}\left(T_e^0\right)} \quad ; \text{ for } T_c \leq T \leq T_e^0 \tag{8}$$

As stated, Ω^0 is applicable to the modelling of the effect of graphitization heat treatment for both graphitizable and non-graphitizable carbons as long as Eq. (2) is deemed a valid approximation. However, if for some reason the d_{002} decrease in LMOs is low enough to be on par with the potential limited decrease of d_{002} in mGBs, Eq. (2) would not be respected. While this should never be the case for graphitizable carbons (where graphitization of LMOs is always significant), it could explain possible deviations between the present model calculations and experimental measurements for some non-graphitizable carbons.

So far, the present mathematical development offers the possibility of modelling the function $d_{002}(T)$ between T_i^0 and T_e^0 by computing Equations (7) and (8) with three independent variables: $d_{002}(T_\alpha)$, $d_{002}(T_\beta)$ and $d_{002}(T_e^0)$. T_α and T_β are two arbitrarily selected temperatures in the range T_i^0 to T_c. However, the number of required independent variables can be reduced from three to two if a second *Ansatz* is introduced:

Ansatz 2 (Eq. (9)): "As the merging and flattening process (Fig. 3b) and the residual healing process (Fig. 3d) are interlinked, $d_{002}(T_e^0)$ is a function of both $d_{002}(T_\alpha)$ and $d_{002}(T_\beta)$, where $T_i^0 < T_\alpha < T_c$ and $T_i^0 < T_\beta < T_c$."

$$d_{002}\left(T_e^0\right) = f\left(d_{002}(T_\alpha), d_{002}\left(T_\beta\right)\right) \tag{9}$$

The following discussion details the physical reasoning needed to develop Eq. (9). First, two new variables (δ_{002} and κ) must be defined with Equations (10) and (11):

$$\delta_{002} = d_{002}(T_\alpha) - d_{002}\left(T_\beta\right) \tag{10}$$

$$\kappa = \frac{N_{ATD}(T_c)}{N_{NAD}(T_c)} = \frac{d_{002}(T_c) - d_{002}\left(T_e^0\right)}{d_{002}\left(T_e^0\right) - d_{002,graphite}} \tag{11}$$

In Eq. (11), $N_{ATD}(T_c)$ and $N_{NAD}(T_c)$ are respectively the number of ATDs and NADs present at T_c, following merging and flattening. $d_{002,graphite}$ is the interlayer spacing of perfect graphite ($d_{002,graphite} = 0.3354$ nm). The arbitrarily defined values for T_α and T_β are respectively 2073 K and 2400 K. In theory, any pair of temperatures located between T_1^0 and T_c could have been chosen. However, it was convenient here to select a pair of temperatures coherent with the carbonization/graphitization experimental study which will be presented in Section 3 of the paper. Eq. (11) states that, for a given graphitization heat treatment, the behaviour of the function $d_{002}(T)$, during the residual healing process ($T_c < T < T_e^0$), is constrained by the relative number of lingering ATDs and NADs following heat treatment at T_c. As discussed previously, the annealing of lingering ATDs is the driving force for the change of d_{002} during the residual healing process (as NADs do not anneal and thus will not propel graphitization). On the other hand, the deviation of the limiting d_{002} value ($d_{002}(T_e^0)$), with reference to perfect graphite ($d_{002,graphite}$), is correlated to the relative number of NADs present at T_c (NADs being located in mGBs i.e. the light grey area in Fig. 1a). In the present model, NADs are not annealed by either the merging and flattening process or the residual healing process, as it was assumed that the high activation energy for said annealing is too high to entail an efficient removal of these defects through heat treatment (under normal conditions). Therefore, NADs act as some kind of implicit graphitization limiter per the present graphitization mechanism (Section 2.2). Some key consequences of Eq. (11) are as follows:

- If $N_{NAD}(T_c)$ is significantly larger than $N_{ATD}(T_c)$: Eq. (11) yields $d_{002}(T_c) \sim d_{002}(T_e^0)$. As the number of graphitization limiters (NADs) is much higher than the number of lingering ATDs, the change in d_{002} by the residual healing process ($T_c < T < T_e^0$) under this condition is a flat line (i.e. no change in d_{002} occurs between T_c and T_e^0).
- If $N_{ATD}(T_c)$ is significantly larger than $N_{NAD}(T_c)$: Eq. (11) yields $d_{002}(T_e) \sim d_{002,graphite}$. This scenario is only possible if ATDs are generated by the merging and flattening process and if L^{LMO} (Fig. 1a) is large. Indeed, the number of ATDs relative to the NADs is akin to a surface/volume ratio for the LMOs as NADs are generated at the LMO surface. A large L^{LMO} yields a low surface/volume ratio and thus increases the relative presence of any lingering ATDs at T_c (compared to the presence of NADs) under the condition that lingering ATDs are indeed present (which is not always the case). Eq. (11) is thus in agreement with the findings of Oberlin [27] which states that large L^{LMO} values are a key feature of high graphitizability carbons.

Knowing that $d_{002}(T_c)$ can be calculated as a function of δ_{002} by a simple rearrangement of Eq. (7), Eq. (9) is rewritten as follows:

$$\kappa = f(\delta_{002}) \tag{12}$$

Eq. (12) is the crux of *Ansatz 2*. The exact form of Eq. (12) is unknown for the moment. However, it is known that it should possess one fundamental mathematical property (Eq. (13)):

$$\kappa(\delta_{002} = 0) = 0 \tag{13}$$

Eq. (13) implies that, if no merging and flattening occurs between T_i^0 and T_c (i.e $\delta_{002} = 0$), the number of ATDs present at T_c relative to the number of NADs will be equal to 0. NADs are present at T_c, even if no merging and flattening occurs because these defects are intrinsic to the presence of mGBs between neighbouring LMOs. mGBs are created as soon as the LMO solidifies at the end of primary carbonization [18]. For example, lets consider the case where primary carbonization (or some other high temperature process involving the pyrolysis of carbon rich gaseous species) yields a non-graphitic carbon whose $L_a = L^{LMO}$. This specific carbon would generate no ATD during merging and flattening as no merging and flattening would occur during heat treatment (the LMO is a single coke crystallite). However, NADs would still be present at T_c due to the presence of mGBs between the single crystallite LMO and its neighbouring LMOs. Hence why κ, for this specific limiting scenario, would be null (therefore why Eq. (13) is needed).

Eq. (13) is insufficient on its own to further develop Eq. (12). Invoking *Ansatz 1*, Eq. (14) is written to further develop the interdependence between κ and δ_{002}:

$$\delta_{002} \sim f\left(d_{002,LMOs}(T_\alpha) - d_{002,LMOs}\left(T_\beta\right)\right) \tag{14}$$

Eq. (14) states that δ_{002} is solely a function of the structural changes in the LMOs during the merging and flattening process (remembering that $T_i^0 < T_\alpha < T_c$ and $T_i^0 < T_\beta < T_c$). Hence, δ_{002} is an implicit measurement of the extent of the reorganisation of the LMOs during the merging and flattening process. Precisely, the extent of the merging and flattening process provides some indirect evaluation of the activation energy for the annealing of ATDs, the assumed graphitization vector of the present model. As stated, ATDs are generated by merging and flattening process and can anneal during merging and flattening, residual healing or both processes, depending on the activation energy of their annealing mechanism. If the activation energy of said ATDs is low, they are relatively mobile and have a high probability to anneal during the relatively low temperature merging and flattening process. Thus, in that case, the reorganisation by merging and flattening is significant. If the activation energy is moderately high, they are relatively stiff defects which will require higher temperature to anneal (i.e. the high temperature residual healing process). Two scenarios, which will serve as a basis for the detailed development of Eq. (12), are proposed for the physical modelling of the link between the merging and flattening process and the residual healing process:

- Low δ_{002}: The reorganisation of the structure is relatively weak. ATDs are generated but the activation energy for their annealing is too high for significant annealing (i.e. flattening) to occur

during merging and flattening. Conceptually, the process generates more ATDs than it consumes. Hence, this reorganisation will yield lingering ATDs at T_c. The amount depends on the magnitude (value of δ_{002}) of the merging and flattening process. This implies that higher δ_{002} values result in an increased number of lingering ATDs at T_c. As the reorganisation by merging and flattening is weak, further transformation by graphitization heat treatment will require higher temperatures for the annealing of high activation energy lingering ATDs (i.e. the residual annealing process).

- High δ_{002}: The reorganisation of the structure is significant. ATDs are generated and subsequently consumed to sustain the reorganisation of the carbon structure by merging and flattening. This behaviour is typical of ATDs with low activation energy for their annealing process. As most ATDs are consumed, few lingering ATDs will remain at T_c. Higher δ_{002} values (associated to a higher reorganisation) will further lower the number of lingering ATDs at T_c as more ATDs are consumed to fuel the reorganisation process. As the merging and flattening process consumed most ATDs, further transformation of the structure by the residual healing process during graphitization heat treatment will be relatively weak.

It is proposed to model the two behaviours (low δ_{002} and high δ_{002}) with a critical first-order non-homogeneous differential model. To do so, two new quantities are defined: δ_c and δ_r. δ_c is a critical threshold which marks the change from the low reorganisation behaviour (low δ_{002}), where ATDs are generated but not significantly consumed, to the high reorganisation behaviour (high δ_{002}), where ATDs are simultaneously generated and consumed. δ_r is the dimensionless reduced δ_{002} and is calculated with Eq. (15):

$$\delta_r = \frac{\delta_{002}}{\delta_c} \tag{15}$$

A third *Ansatz* defines the mathematical form of the first-order non-homogeneous differential model for Eq. (12) considering that this model is actually composed of two functions (one for the low reorganisation behaviour and one for the high reorganisation behaviour):

Ansatz 3: "The merging and flattening process is mathematically modelled with two differential equations in order to account for the change in the annealing behaviour of the ATDs generated by this transformation (Eq. (16) for low δ_{002}, Eq. (17) for high δ_{002})."

$$\frac{1}{\kappa}\frac{d\kappa}{d\delta_r} = \frac{m}{\delta_r} + \frac{n}{|\delta_r - 1|} \quad ; \text{ for } 0 \le \delta_r < 1 \tag{16}$$

$$\frac{1}{\kappa}\frac{d\kappa}{d\delta_r} = \frac{m}{\delta_r} - \frac{n}{|\delta_r - 1|} \quad ; \text{ for } \delta_r > 1 \tag{17}$$

In Equations (16) and (17), two contributions are taken into account: the merging contribution and the flattening contribution. The merging contribution is modelled with a reciprocal function (m/δ_r) of dimensional order m. The flattening contribution is modelled with a critical reciprocal dependence as a function of the difference between δ_r and unity. n is the dimensional order of the flattening contribution of the merging and flattening process. For a low reorganisation process (Eq. (16)), the flattening contribution generates more ATDs than it consumes. Hence, the flattening contribution is positive. For a high reorganisation process (Eq. (17)), the flattening contribution generates and consumes ATDs. The flattening contribution is thus negative. Integrating Eq. (16) yields Eq. (18). Integrating Eq. (17) also lead to the same result. Eq. (18) is valid for both the low and the high reorganisation modes of the merging and flattening process:

$$\kappa = \frac{C_1 \delta_r^m}{|\delta_r - 1|^n} \quad ; \text{ for } \delta_r \ge 0 \tag{18}$$

In Eq. (18), C_1 is a proportionality constant which originated from the integration operation. Henceforward, Eq. (18) is considered as the final form of Eq (12). To reach this result, *Ansatz 1* (Eq. (14)), *Ansatz 2* (Eq. (12)) and *Ansatz 3* (Equations (16) and (17)) were required. As the flattening process is assumed to be three-dimensional (flattening through the thermal annealing of local ATDs is indeed a strong prerequisite for graphitic ordering), and assuming the merging process as a single direction vectorial process, the simplest approach is to define n as equal to 3 and m as equal to 1. Both C_1 and δ_c can be derived from the mathematical analysis [19] of experimental data [11]. Having previously defined $T_\alpha = 2073$ K and $T_\beta = 2400$ K, analysis on the graphitization heat treatment data of Monthioux [11] on some heavy petroleum products (asphalts) results in $C_1 = 0.043$ and $\delta_c = 0.0012$ nm. Theoretically, these values for C_1 and δ_c should apply to all graphitizable and non-graphitizable carbons. They should not be limited to the carbons of Monthioux [11]. This will be verified later in Section 2.4 for the case of graphitizable carbons and Section 2.5 for the case of non-graphitizable carbons.

In light of the previous mathematical development, it can be concluded that the complete ($T_i^0 < T < T_e^0$) function $d_{002}(T)$ can be computed as a function of $d_{002}(T_\alpha)$ and $d_{002}(T_\beta)$ by combining Equations (4), (5), (7), (8) and (18). Validation of the model for the complete graphitizability spectrum will be presented in Sections 2.4 and 2.5. To help the discussion regarding what constitutes a graphitizable or a non-graphitizable carbon, the Ultimate Graphitizability (η_g) of a carbon is arbitrarily defined here with Eq. (19):

$$\eta_g = e^{-\left(\frac{d_{002}(T_e^0) - d_{002,graphite}}{d_{002,turbo} - d_{002,graphite}}\right)} \tag{19}$$

In Eq. (19), $d_{002,turbo}$ is the interlayer spacing of a turbostratic [2] coke crystallite ($d_{002,turbo} = 0.344$ nm). For a perfectly graphitizable carbon ($d_{002}(T_e^0) = d_{002,graphite}$), $\eta_g = 1$. The less graphitizable a carbon is, the more η_g will asymptomatically approach the null value. In order to clarify graphitizability in further discussions, a carbon will be non-graphitizable if $\eta_g < 0.5$ and graphitizable if $0.9 < \eta_g < 1$. Semi-graphitizable carbons will be characterized by $0.5 < \eta_g < 0.9$. η_g highlights the importance of no longer perpetuating the old dichotomy of graphitizable and non-graphitizable carbons as graphitizability is a spectrum, not a binary state. η_g is a suitable descriptor of graphitizability as it respects the three key conditions of this property: graphitizability is a continuous spectrum [11,18], perfect graphitizability is a bounded mathematical limit ($\eta_g = 1$), non-graphitizability is an asymptotic mathematical quantity ($lim_{d_{002}(T_e^0) \to \infty} \eta_g = 0$). Important to note, η_g is an empirical expression which aims solely at facilitating the distinction between graphitizable and non-graphitizable carbons. Hence, η_g should not be compared to the probability of finding a pair of graphite-ordered layers (P_1) as defined by Oberlin [9], which is obtained from the modulation of the 11 band, as the physical significance of both descriptors is entirely different.

2.4. Validating the model for the case of graphitizable carbons

Prior to discussing the application of the model, Tables 1 and 2 respectively summarize the various parameters of the present graphitizability formalism. It is relevant to highlight that the present graphitizability model is constructed solely with five

fundamental parameters (β, γ, T_c, m, n), all of them possessing some physical basis. The two independent variables of the model are $d_{002}(T_\alpha)$, $d_{002}(T_\beta)$. The other parameters are either calculated from intrinsic mathematical properties of the present model (T_i^0, T_e^0, θ_c) or derived from available experimental data (δ_c, C_1). Specifically, δ_c and C_1 were calculated solely based on the data of Monthioux [11]. The values of δ_c and C_1 parameters were taken as transferable, without any adjustment, to the calculation of the $d_{002}(T)$ function of all other graphitizable and non-graphitizable carbons [2,5,9,25,42–64] studied in the present paper. Another important point, the model error is dependent on the uncertainty of the fundamental critical temperature [19] (T_c) and on the error when measuring independent variables $d_{002}(T_\alpha)$ and $d_{002}(T_\beta)$. For the moment, the sensitivity analysis of the model will be limited to the error on T_c. Fig. 4 presents the algorithm of calculation of the present graphitizability model which produces the function $d_{002}(T)$. This function is applicable to the modelling of graphitizable and non-graphitizable carbons as discussed in Section 2.3. This section of the paper will discuss solely the case of graphitizable carbons.

Figs. 5–7 present the results of the model for some typical graphitizable carbons. The experimental error on d_{002} measurements for such carbons ranges from 2×10^{-4} nm, at best [65], to the upper value [19] of 5×10^{-4} nm. An intermediate value of 3.5×10^{-4} nm is thus considered for the present comparative analysis. Application of the model to other graphitizable carbons [9,42–56] yielded results of similar quality as the ones of Figs. 5–7. Figs. 8 and 9 provides further insight on the inner working of the function $d_{002}(T)$. Specifically, Fig. 8 presents a typical case of a merging and flattening process where the low magnitude of δ_{002} ($\delta_{002} < \delta_c$) promotes the formation, but not the subsequent annealing, of ATDs between T_i^0 and T_c. Thus, a high number of lingering ATDs will be present at T_c. Said lingering ATDs anneal at higher temperature by the residual healing process ($T_c < T < T_e^0$), hence the sigmoid-shaped curve of $d_{002}(T)$. Fig. 9, on the other hand, is representative of a merging and flattening process of high magnitude ($\delta_{002} > \delta_c$). In this mode of the process, ATDs are generated and subsequently annealed during merging and flattening. Hence, very few lingering ATDs will be present at T_c. Thus, the structural changes during the residual healing step (which are driven by the consumption of lingering ATDs) will be minor. In that case, the shape of the function $d_{002}(T)$ between T_c and T_e^0 approaches a flat line.

Comparing Figs. 8 and 9 highlights a possible deviation between the model calculations and the experimental d_{002} measurements in the low temperature region of Fig. 9. This is a consequence of a fundamental limitation of the model. In this temperature region of the merging and flattening process (between T_i^0 and $\sim$ 2073 K), almost all chemically bonded heteroatoms [23,66] are released from the carbon structure by the heat treatment process. This promotes a more extensive (relative to a pure carbon material) merging and flattening process. As the present model assumes pure carbon structures (no heteroatoms are present), deviations are to be expected if the graphitization heat treatment was somehow enhanced by the release of heteroatoms in this temperature region. However, once all heteroatoms are removed, the experimental measurements and the model should be in agreement as the energetics of the graphitization heat treatment process would no longer be enhanced by the phenomena of heteroatom release. This is the case in Fig. 9 for T greater than $\sim$ 2073 K. Further discussion on the effect of heteroatom release on general graphitization behaviour is beyond the scope of the present paper.

A Nash-Sutcliffe coefficient [67] (NS) evaluates the prediction quality of the model (assuming $T_c = 2550$ K) for all studied graphitizable carbons [2,5,9,11,42–54,56–58]. A value of 1 for the NS coefficient signifies a perfect correspondence between the experimental data and the model calculations. The NS coefficient ranges from 1 (ideal) to $-\infty$ (no match). For 2073 K $< T < T_e^0$, the model yields for the selected data on graphitizable carbons NS = 0.99. For $T_i^0 < T < T_e^0$, NS = 0.97. As discussed previously, this decrease in precision between the two temperature ranges originates from the effect of heteroatom release between T_i^0 and 2073 K which modifies the energetic of the merging and flattening process relative to the pure carbon path (i.e. the present model).

Assuming $T_c = 2550$ K, Fig. 10 presents the sensitivity analysis of the model for the independent variables $d_{002}(T_\alpha)$ and $d_{002}(T_\beta)$ considering a typical error [19,65] on d_{002} measurements of $\pm 3.5 \times 10^{-4}$ nm. Comparison between Figs. 8 and 10 shows that η_g is more sensitive to the measurement of $d_{002}(T_\alpha)$ and $d_{002}(T_\beta)$ than the choice of T_c value. Thus, to predict η_g with the best confidence, the methodology of Iwashita [65] for the measurement of d_{002} is recommended as the precision of this method is, at best, $\pm 2 \times 10^{-4}$ nm.

2.5. Applying the model to some non-graphitizable carbons

Section 2.3 claimed that the present model (Fig. 4) can be applied to non-graphitizable carbon under the condition that Eq. (1) is respected. This will be verified here. However, as stated in Section 2.3, it should be noted that for some specific non-graphitizable carbons, the low reorganisation of the LMOs may be on par with the (potential) low reorganisation of the mGBs. Hence, for these carbons, Eq. (1) may not be applicable. However, even if this were to be the case, the model should still be a reasonable estimation of the graphitization function ($d_{002}(T)$), albeit with a more important modelling error. Indeed, for most carbons, the main contributors to $d_{002}(T)$ should always be the LMOs. Important to note, as the same critical exponents were used to model graphitization heat treatment in both non-graphitizable and graphitizable carbons, it is implied that the local nature of ATDs being annealed in both processes is the same. Figs. 11–13 present key results which illustrates how the model can predict the graphitization function of some non-graphitizable carbons as a function of $d_{002}(T_\alpha)$ and $d_{002}(T_\beta)$.

In Figs. 11–13, similar to what could be understood from comparing Figs. 8 and 9 in Section 2.4, non-negligible deviations between the model calculations and the experimental results are observed in the range T_i^0 to $\sim$ 2073 K. As discussed in Section 2.4, these deviations can be explained by the release of heteroatoms in

Table 1
Fundamental parameters of the present graphitizability model.

Parameter	Value	Justification
β	-0.2	Typical value of an Heisenberg-type critical transition with three degrees of freedom [68].
γ	0.8	Temperature ratio which constrains the change from quasi-linearity to non-linearity [19] of the function $d_{002}(T)$.
T_c	2550±50 K	Expected thermodynamic value of the graphitization temperature threshold as calculated by the surface energy models of Abrahamson [69] and Ouzilleau [23].
m	1	Dimensional order of the merging contribution for the modelling of the merging and flattening process by Equations (16) and (17) (Section 2.3).
n	3	Dimensional order of the flattening contribution for the modelling of the merging and flattening process by Equations (16) and (17) (Section 2.3).

Table 2
Calculated parameters of the present graphitizability model $d_{002}(T) = f(d_{002}(T_\alpha), d_{002}(T_\beta))$ where $T_\alpha = 2073$ K and $T_\beta = 2400$ K.

Parameter	Value	Justification
T_i^0	1715±35 K	Derived from the following fundamental property [7] of Ω^0: $\frac{d(\Omega^0[T_i^0])}{dT} = 0$.
T_e^0	3385±65 K	Calculated according to the temperature symmetry (Section 2.3) of Ω^0 ($T_c - T_i^0 = T_e^0 - T_c$).
θ_c	$-3.83 \times 10^{-3} \pm 7.5 \times 10^{-5}$	Derived from the following fundamental property [7] of Ω^0: $\Omega(T_c) = 0$.
δ_c	1.2×10^{-3} nm	Critical parameter derived from the experimental function $\kappa(\delta_r)$ which was empirically [19] obtained from the data of Monthioux [11] (Section 2.3).
C_1	0.043	Proportionality constant of Eq. (18) (Section 2.3) obtained from the experimental function $\kappa(\delta_r)$ which was empirically [19] obtained from the experimental data of Monthioux [11].

1. Initialisation:
   - Set $d_{002}(T_\alpha)$.
   - Set $d_{002}(T_\beta)$.
   - Set T.
2. Calculate:
   - δ_{002} with Eq. 10.
   - δ_r with Eq. 15.
   - κ with Eq. 18.
   - $d_{002}(T^0{}_i)$ and $d_{002}(T_c)$ by solving the binary equation system $[\Omega^0(T_\alpha); \Omega^0(T_\beta)]$, where Ω^0 is calculated with Eq. 7.
   - $d_{002}(T^0{}_e)$ with κ and $d_{002}(T_c)$.
3. If $T^0{}_i \leq T \leq T_c$:
   - Calculate $d_{002}(T)$ with Equations 4 and 7.
4. If $T_c \leq T \leq T^0{}_e$:
   - Calculate $d_{002}(T)$ with Equations 5 and 8.

Fig. 4. Algorithm of calculation for the function $d_{002}(T)$ of graphitizable and non-graphitizable carbons as a function of $d_{002}(T_\alpha)$ and $d_{002}(T_\beta)$ where $T_\alpha = 2073$ K, $T_\beta = 2400$ K and $T_c = 2550$ K.

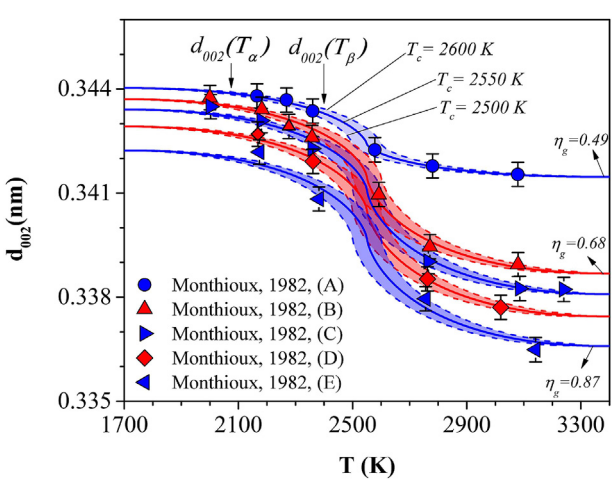

Fig. 5. Comparison between the experimental measurements of Monthioux [11] and the d_{002} calculated as a function of $d_{002}(T_\alpha)$ and $d_{002}(T_\beta)$ by the present graphitizability model (Fig. 4) where $T_\alpha = 2073$ K and $T_\beta = 2400$ K. η_g is calculated with Eq. (19). The lens shape of the results (light red or light blue) illustrates the sensitivity due to $T_c = 2550 \pm 50$ K. The typical experimental error [19,65] on d_{002} measurements is taken as 3.5×10^{-4} nm. Studied carbons: (A) Asphalt Athabasca 1, (B) Asphalt Emeraude, (C) Asphalt Batiraman, (D) Asphalt Mandgi, (E) Asphalt Athabasca 2. (A colour version of this figure can be viewed online.)

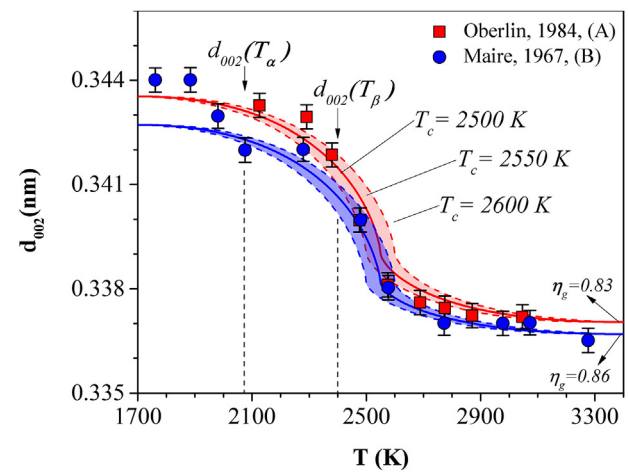

Fig. 6. Comparison between the experimental measurements of Oberlin [5], Maire [57] and the d_{002} calculated as a function of $d_{002}(T_\alpha)$ and $d_{002}(T_\beta)$ by the present graphitizability model (Fig. 4) where $T_\alpha = 2073$ K and $T_\beta = 2400$ K. η_g is calculated with Eq. (19). The lens shape of the results illustrates the sensitivity due to $T_c = 2550 \pm 50$ K. The typical experimental error [19,65] on d_{002} measurements is taken as 3.5×10^{-4} nm. Studied carbons: (A) Coal tar pitch, (B) Polyvinyl chloride. (A colour version of this figure can be viewed online.)

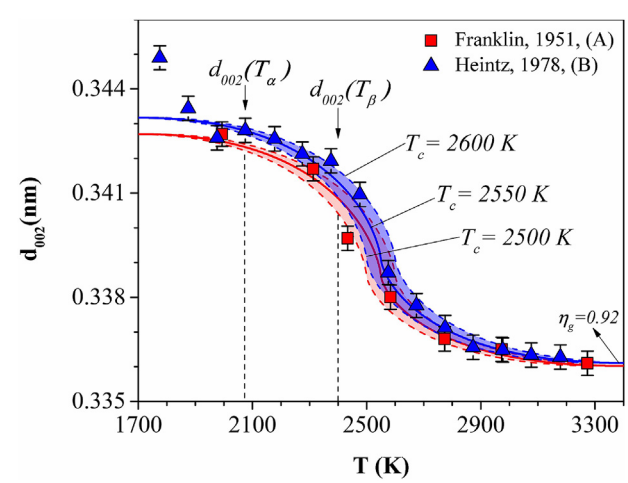

Fig. 7. Comparison between the experimental measurements of Franklin [2], Heintz [58] and the d_{002} calculated as a function of $d_{002}(T_\alpha)$ and $d_{002}(T_\beta)$ by the present graphitizability model (Fig. 4) where $T_\alpha = 2073$ K and $T_\beta = 2400$ K. η_g is calculated with Eq. (19). The lens shape of the results illustrates the sensitivity due to $T_c = 2550 \pm 50$ K. The typical experimental error [19,65] on d_{002} measurements is taken as 3.5×10^{-4} nm. Studied carbons: (A) Polyvinyl chloride, (B) Petroleum coke. (A colour version of this figure can be viewed online.)

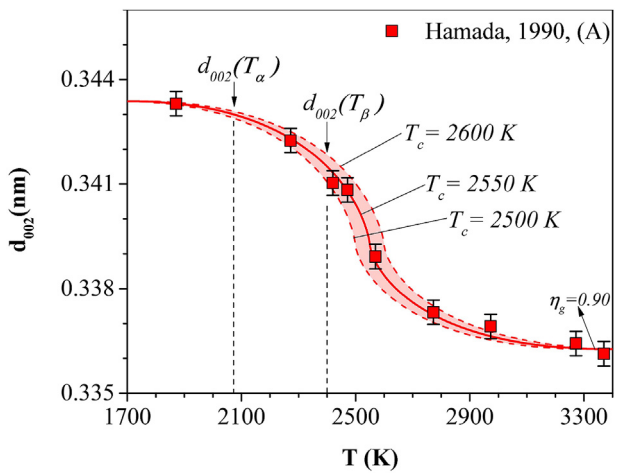

Fig. 8. Comparison between the experimental measurements of Hamada [42] and the d_{002} as a function of $d_{002}(T_\alpha)$ and $d_{002}(T_\beta)$ by the present graphitizability model (Fig. 4) where $T_\alpha = 2073$ K and $T_\beta = 2400$ K. η_g is calculated with Eq. (19). The lens shape of the results illustrates the sensitivity due to $T_c = 2550\pm50$ K. The typical experimental error [19,65] on d_{002} measurements is taken as 3.5×10^{-4} nm. Studied carbon: (A) Carbon fibers. (A colour version of this figure can be viewed online.)

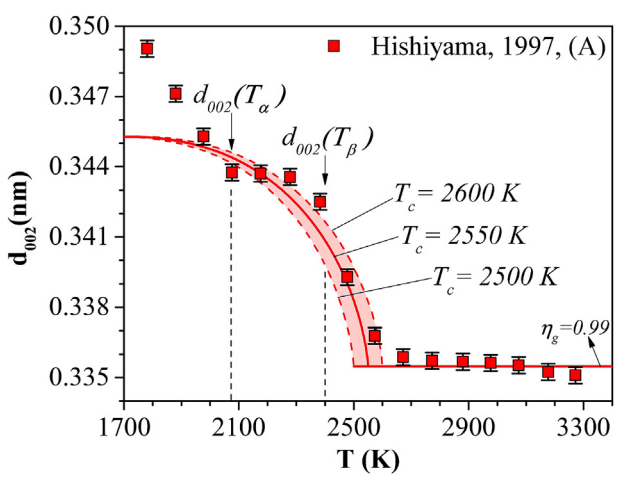

Fig. 9. Comparison between the experimental measurements of Hishiyama [47] and the d_{002} calculated as a function of $d_{002}(T_\alpha)$ and $d_{002}(T_\beta)$ by the present graphitizability model (Fig. 4) where $T_\alpha = 2073$ K and $T_\beta = 2400$ K. η_g is calculated with Eq. (19). The lens shape of the results illustrates the sensitivity due to $T_c = 2550\pm50$ K. The typical experimental error [19,65] on d_{002} measurements is taken as 3.5×10^{-4} nm. Studied carbon: (A) Polyimide film Kapton. (A colour version of this figure can be viewed online.)

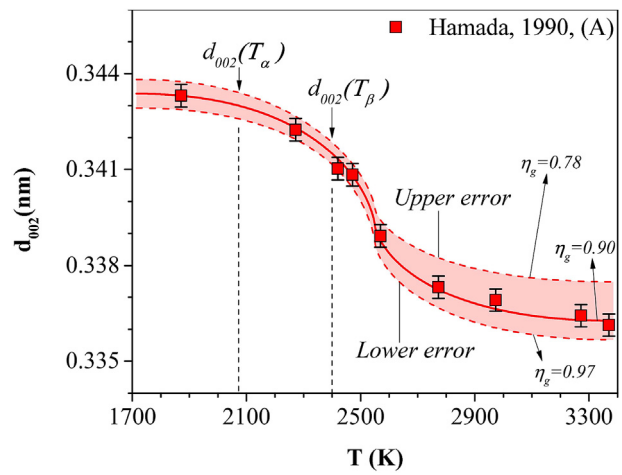

Fig. 10. Sensitivity analysis of the expected error on parameters $d_{002}(T_\alpha)$ and $d_{002}(T_\beta)$, where $T_\alpha = 2073$ K and $T_\beta = 2400$ K, and the model calculations (assuming $T_c = 2550$ K), with comparative analysis to the measurements of Hamada [42]. η_g is calculated with Eq. (19). The lens shape of the results illustrates the sensitivity due to a typical [19,65] error on $d_{002}(T_\alpha)$ and $d_{002}(T_\beta)$ i.e. $\pm3.5 \times 10^{-4}$ nm. Studied carbon: (A) Carbon fibers. (A colour version of this figure can be viewed online.)

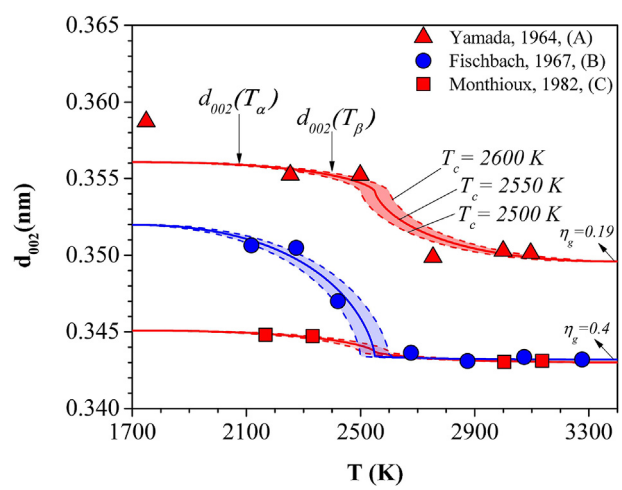

Fig. 11. Comparison between the experimental measurements of Yamada [59], Fischbach [60] and Monthioux [11] and the d_{002} calculated as a function of $d_{002}(T_\alpha)$ and $d_{002}(T_\beta)$ by the present graphitizability model (Fig. 4) where $T_\alpha = 2073$ K and $T_\beta = 2400$ K. η_g is calculated with Eq. (19). The lens shape of the results illustrates the sensitivity due to $T_c = 2550\pm50$ K. Studied carbons: (A) Glassy carbon, (B) Polymer-based glassy carbon, (C) Asphalt R-15 769. (A colour version of this figure can be viewed online.)

this specific temperature range. Indeed, this would modify the energetic pathways of the structural transformation by graphitization heat treatment relative to a pure-carbon energetic pathway was assumed. To evaluate the quality of the predictions of the model in Figs. 11–13, NS coefficients were calculated. NS coefficients ranges from 1 (perfect match) to $-\infty$ (no match). For 2073 K $< T < T_e^0$, applying the model ($T_c = 2550$ K) to the selected data on non-graphitizable carbons yields NS $= 0.98$. For $T_i^0 < T < T_e^0$, NS $= 0.91$.

For all results presented in Figs. 5–10 (graphitizable carbons) and Figs. 11–13 (non-graphitizable carbons), the numerical values of parameters C_1 and δ_c (respectively 0.043 and 1.2×10^{-3} nm) were fixed. As these values were originally calculated from experimental results on graphitized asphalts [11], the fact that these parameters are transferable across many carbons (graphitizable and non-graphitizable) is in agreement with the statements of Oberlin which are that graphitizability is distributed across a spectrum and is the consequence of the cumulative transformation of single units of structure (i.e. LMOs).

3. Experimental carbonization/graphitization study of chemical and structural properties correlated to $d_{002}(T_\alpha)$ and $d_{002}(T_\beta)$ for some graphitizable carbons

3.1. Constructing two phenomenological functions for δ_{002} and $d_{002}(T_\beta)$

Section 2.4 and 2.5 reinforced the validity of the graphitization mechanism of Fig. 3 and its associated physical model (whose algorithm of calculation was detailed in Fig. 4). The key conclusion

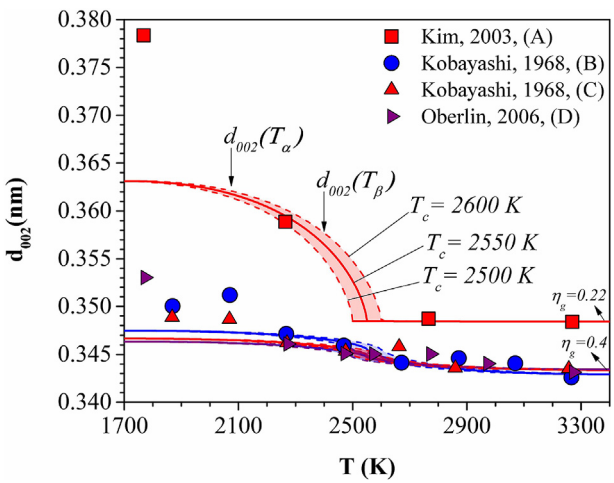

Fig. 12. Comparison between the experimental measurements of Kim [61], Kobayashi [62] and Oberlin [9] and the d_{002} calculated as a function of $d_{002}(T_\alpha)$ and $d_{002}(T_\beta)$ by the present graphitizability model (Fig. 4) where $T_\alpha = 2073$ K and $T_\beta = 2400$ K. η_g is calculated with Eq. (19). The lens shape of the results illustrates the sensitivity due to $T_c = 2550 \pm 50$ K. Studied carbons: (A) Poly (vinylidene chloride), (B) Phenol-formaldehyde resin, (C) 3-Methylphenol-formaldehyde resin, (D) Saccharose coke. (A colour version of this figure can be viewed online.)

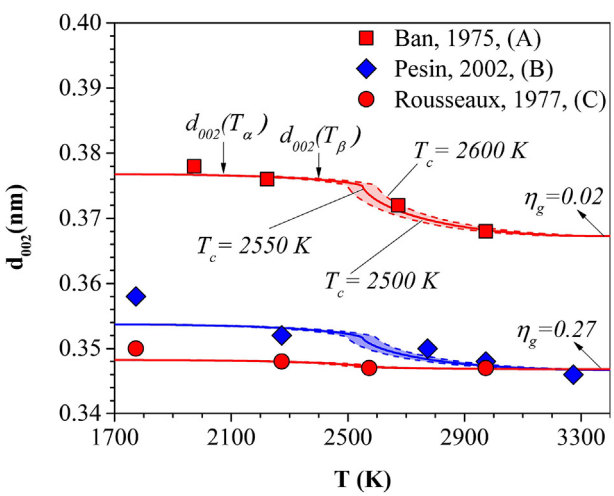

Fig. 13. Comparison between the experimental measurements of Ban [25], Pesin [63] and Rousseaux [64] and the d_{002} calculated as a function of $d_{002}(T_\alpha)$ and $d_{002}(T_\beta)$ by the present graphitizability model (Fig. 4) where $T_\alpha = 2073$ K and $T_\beta = 2400$ K. η_g is calculated with Eq. (19). The lens shape of the results illustrates the sensitivity due to $T_c = 2550 \pm 50$ K. Studied carbons: (A) Poly (vinylidene chloride), (B) Phenol-formaldehyde resin, (C) Furfuryl alcohol glassy carbon. (A colour version of this figure can be viewed online.)

was that, for the studied graphitizable and non-graphitizable carbons, η_g is a function of independent variables $d_{002}(T_\alpha)$ and $d_{002}(T_\beta)$. This function was developed through the combination of Equations (9) and (19). Equivalently, one can rewrite Equations (9) and (19) as Eq. (20):

$$\eta_g = f\left(d_{002}\left(T_\beta\right), \delta_{002}\right) \tag{20}$$

The goal of Section 3 is to improve the scope of Eq. (20) through the phenomenological study of experimental factors correlated to $d_{002}(T_\beta)$ and δ_{002} (i.e. the two fundamental graphitization variables). One can assume that there exist two arbitrary functions (Equations (21) and (22)) which could respectively predict $d_{002}(T_\beta)$ and δ_{002} as a function of some unknown number of independent variables x_i and y_i:

$$d_{002}\left(T_\beta\right) = f(x_1, x_2, x_3, \ldots, x_i) \tag{21}$$

$$\delta_{002} = f(y_1, y_2, y_3, \ldots, y_i) \tag{22}$$

Based on the kinetic studies of Fischbach [4], Fair [44], Hishiyama [47] and Fitzer [70], two independent variables of Equations (21) and (22) can be intuitively proposed: the heating rate (HR) of the carbonization/graphitization process (remembering here that we consider $T = T_{HT}$) and the holding time at maximal temperature (t_{hold}). Both effects are required to model the effect of time on the carbonization and graphitization heat treatment processes. We thus obtain:

$$d_{002}\left(T_\beta\right) = f(\mathrm{HR}, t_{hold}, \ldots, x_i) \tag{23}$$

$$\delta_{002} = f(\mathrm{HR}, t_{hold}, \ldots, y_i) \tag{24}$$

The study of the time dependence of Equations (23) and (24) is beyond the scope of the present work. Thus, the mathematical development of Equations (23) and (24) will be limited to a single well-defined heat treatment process (the pr_1 process) with operating parameters HR_1 and $t_{hold,1}$. It is proposed that Equations (23) and (24) are each respectively defined with only one independent variable (apart from HR_1 and $t_{hold,1}$): the orientation factor W_f for Eq. (23) and the graphitization resistance Ψ for Eq (24). Ψ can be interpreted as some dimensionless force which limits the reorganisation potential of the LMOs during the densification of the IM by the merging and flattening process (Fig. 3b). Equations (23) and (24) simplify to the following:

$$\left[d_{002}\left(T_\beta\right)\right]_{\mathrm{pr}_1} = f\left(W_f\right) \tag{25}$$

$$[\delta_{002}]_{\mathrm{pr}_1} = f(\Psi) \tag{26}$$

Walker [71,72] proposed that the relative intensities of the carbon and silicon 002 X-ray diffraction peaks of a typical (carbon + silicon) powder can serve as a measure of the relative alignment of crystallites in a carbon (i.e. alignment of coke crystallites in Fig. 1b). Hence, W_f is calculated with Eq. (27):

$$W_f = \left(\frac{A_C}{A_{Si}}\right)_{T_{semicoke}} \tag{27}$$

In Eq. (27), A_C is the area under the carbon 002 peak (above background levels) of the diffraction pattern of a given (carbon + silicon) powder sample where that carbon was obtained following primary carbonization [5,18,19] at the heat treatment temperature $T_{semicoke}$ (where $T_{semicoke} \sim 823$ K). A_{Si} is the area under the silicon 002 peak (above background levels) of the diffraction pattern of a given (carbon + silicon) powder sample. As stated, W_f represents the relative alignment of crystallites in LMOs. The silicon serves as reference point for the relative measurement of the unsymmetrical nature of the material. Higher W_f are associated to a more symmetrical carbon material (i.e. the coke crystallites of the LMOs are well mutually oriented). Lower W_f are associated to less oriented carbon materials.

As stated, Ψ is the graphitization resistance of LMOs. The qualitative impact of Ψ on the physical behaviour of the merging and flattening process is as follows:

- Low Ψ: merging and flattening will yield a low number of lingering ATDs at T_c. The maximal concentration of NADs at T_c will be relatively low.
- High Ψ: merging and flattening will yield lingering ATDs at T_c. The maximal concentration of NADs at T_c will be relatively high.

Taking inspiration from the work of Walker [71,72] and Oberlin [5], Ψ is defined with Eq. (28) (for the case of relatively low sulfur carbons):

$$\Psi = \frac{1}{W_f} \cdot \left(\frac{\%O_{at.}}{\%H_{at.}}\right)_{T_{semicoke}} \quad ; \text{ for } \%S_{wt.} < S_{low} \tag{28}$$

In Eq. (28), $\%O_{at.}$ and $\%H_{at.}$ are respectively the atomic percentages of oxygen and hydrogen of a carbon material following heat treatment at $T_{semicoke}$. $\%S_{wt.}$ is the weight percentage of sulfur following heat treatment at $T_{semicoke}$. Ψ is the product of two contributions: W_f (which represents the relative orientation of coke crystallites in LMOs) and the oxygen/hydrogen ratio. For relatively low sulfur carbons ($\%S_{wt.} < S_{low}$ where S_{low} is the lower sulfur content limit for the application of Eq. (28)), Oberlin [5] showed that the specific oxygen/hydrogen composition ratio, following primary carbonization, was strongly correlated to the extent of the LMOs (i.e. L^{LMO}). Higher oxygen/hydrogen ratios are indicative of low L^{LMO} values while low ratios are associated to high L^{LMO}. For carbons with relatively high sulfur contents, it could be necessary to include the contribution of cross-linking sulfur atoms (sulfur present in the mGBs) to improve [18] Eq. (28). Indeed, it was proposed [5,73] that cross-linking sulfur promotes the formation of smaller LMOs, similar to oxygen. Only in the case [5] of very high sulfur carbons would this simplification entail a significant deviation from reality. Kipling [74] proposed a sulfur content limit of $S_{low} \sim 9\%$ (weight) for such a strong deviation (sulfur content measured following heat treatment 700 °C). S_{low} will thus serve as a limit for Eq. (28) until the role of cross-linking sulfur can be better implemented in view of the present graphitization theory. The role of heteroatoms in the calculation of Ψ is radically different than their possible catalytic role during graphitization heat treatment between T_i^0 and 2073 K (Section 2.4). Concerning Ψ, measuring the heteroatom content provides an implicit estimation of L^{LMO}. On the other hand, graphitization between T_i^0 and 2073 K releases residual heteroatoms which lower the energy barrier for the transformation by graphitization heat treatment, relative to the pure carbon transformation.

Regardless of the role of sulfur, the purpose of Eq. (28) is to suggest that Ψ is function of crystallite orientation (W_f) and L^{LMO}, L^{LMO} itself being correlated to the oxygen/hydrogen ratio. Well-oriented crystallites (high W_f) will promote the formation of ATDs with very low activation energies for their thermal annealing process. This translates in greater annealing at lower temperatures compared to less well-oriented crystallites which will form ATDs requiring the higher temperature residual healing process to anneal. Fewer lingering ATDs will persist up to T_c in well-oriented LMOs. Thus, high values of W_f will promote a more important graphitic reorganisation of LMOs (through ATD annealing) during the merging and flattening process ($\delta_r > 1$). On the other hand, low values of W_f will promote graphitic reorganisation of LMOs during the residual healing process. In short, less well-oriented crystallites (low W_f) promote a higher resistance as the topology of the generated ATDs will be relatively more prone to develop curvature (hence their higher annealing activation energy). Higher heat treatment temperatures ($T > T_c$) will thus be needed to anneal the lingering ATDs formed from these somewhat curved defects of the merging and flattening process.

Concerning the effect of L^{LMO}, carbons with low L^{LMO} values will tend to have a high surface/volume ratio for their LMOs. This in turn increases the relative presence of peripheral NADs and limits the maximal potential number of ATDs created during the merging and flattening process. Conceptually, as the relative presence of NADs increases, the lower the probability of forming large LMOs will be. In turn, this decreases the maximal number of ATDs which could potentially be present in the material following heat treatment at T_c. This negative effect on graphitizability can be counteracted upon by an increase of L^{LMO}. The present model is thus in agreement with Oberlin [27] main finding that graphitizable carbons (which usually have high δ_{002} values) have a high average L^{LMO} value.

Sections 3.2, 3.3 and 3.4 will present the carbonization/graphitization experimental results for the development of the two phenomenological functions of the present approach (Equations (25) and (26)). The associated mathematical development of each function will also be discussed. The methodology to obtain said experimental data is detailed in Section 3.2. The present experimental study will be limited to the case of some graphitizable carbons.

3.2. Experimental method

The graphitizable carbons consist of 6 petroleum cokes (which have yet to complete their primary carbonization process) and 5 coal tar pitches. The cokes are identified as C1, C2, C3, C4, C5, C6 and the pitches as P1, P2, P3, P4, P5. All carbon materials were sequentially heat treated at $T_{semicoke}$ (i.e. 823 K), T_α (i.e. 2073 K) and T_β (i.e. 2400 K). HR_1 was equal to ~ 4 °Cmin^{-1}. This HR_1 value was selected as the experiments of Bonnamy [14] showed that it resulted in $T_{semicoke} \sim 823$ K (for most graphitizable pitches and cokes). The heating rate was the same for all heat treatments ($T_{semicoke}$, T_α, T_β). This specification is needed for the heat treatments at T_α and T_β to respect the simplification which yielded Equations (25) and (26) from Equations (23) and (24). The holding time at maximal temperature ($t_{hold,1}$) was chosen at 10 min to emulate the graphitizability experiments of Monthioux [11]. $t_{hold,1}$ was also maintained constant for all heat treatments. These parameters (HR_1 and $t_{hold,1}$) define our heat treatment process pr_1 (i.e. the pr_1 conditions). Following heat treatment at $T_{semicoke}$, the oxygen, hydrogen and sulfur contents of all carbons were measured by LECO®combustion analysis. For carbons heat treated at $T_{semicoke}$, T_α and T_β, the X-Ray Diffraction (XRD) patterns were obtained following the standard methodology of Iwashita et al. [65,75]. Mixtures of 80% (weight fraction) carbon sample and 20% (weight fraction) standard silicon were chosen for all XRD measurements. As detailed by Iwashita, raw XRD patterns were corrected for the Lorentz factor, the polarization factor, the absorption factor, the atomic scattering factor and for the background contribution. From the corrected XRD patterns, A_c and A_{Si} are respectively calculated by fitting the 002 "peak" (the word peak is loosely appropriate here as it is not a peak per se) of carbon and the reference silicon peak with individual Voigt functions. W_f is subsequently calculated with Eq. (27). Fig. 14 provides an example of a typical diffraction pattern for the calculation of the W_f parameter of coke C1. $d_{002}(T_\alpha)$ and $d_{002}(T_\beta)$ values of each sample were extracted from the respective corrected XRD patterns of carbons following heat treatment at T_α and T_β.

3.3. Misorientation class model for $d_{002}(T_\beta)$ as a function of W_f

Tables 3 and 4 present the measured values of W_f and $d_{002}(T_\beta)$ following heat treatment of the petroleum cokes (C1, C2, C3, C4, C5, C6) and the pitches (P1, P2, P3, P4, P5). Some hypothesis are needed to develop Eq. (25) from this experimental data. First, carbons are considered to be classified based on criteria of (relatively) similar

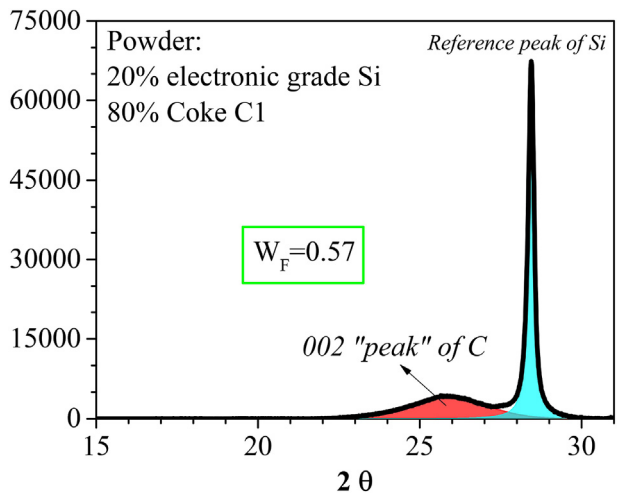

Fig. 14. Corrected diffraction pattern of a powder mixture containing 80% (wt.) carbonized coke C1 obtained following heat treatment at $T_{semicoke}$ (where $T_{semicoke}$ = 823 K) and 20% (wt.) electronic grade silicon. W_f is calculated with Eq. (27), where A_c is equal to the area in red and A_{Si} is equal to the area in light blue. (A colour version of this figure can be viewed online.)

LMO size (L^{LMO} in Fig. 1a). The idea of a classification system based on L^{LMO} has been previously discussed by Oberlin [18]. In the present case, as graphitizable petroleum cokes and graphitizable coal tar pitches both typically [5,9,18,27] develop 50 nm < L^{LMO} < 100 nm, it is assumed that they belong to the same class of carbon materials (Class 7 according to Oberlin [18]). This implies Eq. (29):

$$\left(L^{LMO}\right)_{C1} \sim \ldots \sim \left(L^{LMO}\right)_{C6} \sim \left(L^{LMO}\right)_{P1} \sim \ldots \sim \left(L^{LMO}\right)_{P5} \quad (29)$$

Important to note, Eq. (29) only states that the L^{LMO} of the studied carbons (C1, C2, C3, C4, C5, C6, P1, P2, P3, P4, P5) are relatively similar when compared to the L^{LMO} of other carbon classes (e.g. the important difference [7] between the L^{LMO} of graphitizable and non-graphitizable carbons). Next, it is supposed that there exists, for a given class of carbons heat treated at T_β, a function which calculates some statistical average distance (defined as $L_1(T_\beta)$) between the coke crystallites of LMOs as a function of the average misorientation degree of said LMOs (defined with $(W_f)^{-1}$). $L_1(T_\beta)$ is developed in the final stages of the mesophase solidification process (i.e. just prior to the end of primary carbonization). In theses final stages, the order of the LMOs is close to final, but individual crystallites still retain some mobility. For highly oriented materials (relatively large value for W_f), the developed $L_1(T_\beta)$ is minimal ($L_1(T_\beta) \sim L_1(T_\beta)_{min}$). Increasing misorientation results in a larger $L_1(T_\beta)$ (relative to the minimum value) due to the more important contribution of atomic repulsion between misoriented coke crystallites. However, there exists some peak value of W_f (W_c) where any further increase in misorientation will actually lower $L_1(T_\beta)$ due to the anisotropic nature of the graphenic structure of coke crystallites which implies reduced repulsion at a very high misorientation (low W_f). The value for $L_1(T_\beta)$ is set when the material solidifies at the semicoke stage. All in all, it is stated that the samples of Tables 3 and 4 belong to a *misorientation class* named G7(pr$_1$) (Class 7 LMOs heat treated under pr$_1$ conditions). This class is characterized by 0.45 < W_f < 0.85 and 50 nm < L^{LMO} < 100 nm. As stated in Section 3.2, it is produced with the following pr$_1$ process: HR$_1$ ~ 4 °Cmin^{-1} and $t_{hold,1}$ = 10 min. For the present misorientation class G7(pr$_1$), a simple peak function (Eq. (30)) models the anisotropic repulsion phenomena:

Table 3
Measured values of the interlayer spacing $d_{002}(T_\beta)$ and the relative orientation of coke crystallites in LMOs (W_f). All values for the measured properties were obtained from the XRD patterns of various green petroleum cokes (C1, C2, C3, C4, C5, C6) following heat treatment under pr$_1$ conditions. W_f was calculated with Eq. (27) for carbons heat treated at $T_{semicoke}$ ($T_{semicoke}$ = 823 K). The value of T_β was arbitrarily defined as 2400 K in Section 2.3. The experimental error [65] on $d_{002}(T_\beta)$ measurements is, at best, 2 × 10^{-4} nm. The measured error on W_f is ~ 0.03.

	C1	C2	C3	C4	C5	C6
Measured property						
W_f	0.57	0.8	0.62	0.6	0.71	0.64
$d_{002}(T_\beta)$ (nm)	0.3406	0.3400	0.3399	0.3400	0.3399	0.3398

Table 4
Measured values of the interlayer spacing $d_{002}(T_\beta)$ and the relative orientation of coke crystallites in LMOs (W_f). All values for the measured properties were obtained from the XRD patterns of various coal tar pitches (P1, P2, P3, P4, P5) following heat treatment under pr$_1$ conditions. W_f was calculated with Eq. (27) for carbons heat treated at $T_{semicoke}$ ($T_{semicoke}$ = 823 K). The value of T_β was arbitrarily defined as 2400 K in Section 2.3. The experimental error [65] on $d_{002}(T_\beta)$ measurements is, at best, 2 × 10^{-4} nm. The measured error on W_f is ~ 0.01.

	P1	P2	P3	P4	P5
Measured property					
W_f	0.5	0.52	0.52	0.52	0.47
$d_{002}(T_\beta)$ (nm)	0.3414	0.3413	0.3413	0.3414	0.3413

$$\left[L_1\left(T_\beta\right) - L_1\left(T_\beta\right)_{min}\right]_{pr_1} = B_1 \frac{S_1\left(e^{-B_1\left(\frac{W_c}{W_f}-1\right)}\right)}{\left(1+e^{-B_1\left(\frac{W_c}{W_f}-1\right)}\right)^2} \quad ; \text{ for } 0.45 < W_f < 0.85 \quad (30)$$

In Eq. (30), S_1 and B_1 are fitting parameters which models Eq. (30) for the G7(pr$_1$) class of carbons. According to the present approach, for a given mistorientation class, the increase in $d_{002}(T_\beta)$ relative to the minimal value at ideal orientation ($d_{002}(T_\beta)_{min}$) is due to the average increase of $L_1(T_\beta)$ relative to $L_1(T_\beta)_{min}$. Hence, this variation in $d_{002}(T_\beta)$ can be calculated as a function of W_f with Eq. (31):

$$\left[d_{002}\left(T_\beta\right) - d_{002}\left(T_\beta\right)_{min}\right]_{pr_1} = \int_{\infty}^{W_f} \left[L_1\left(T_\beta\right) - L_1\left(T_\beta\right)_{min}\right]_{pr_1} dW_f \quad (31)$$

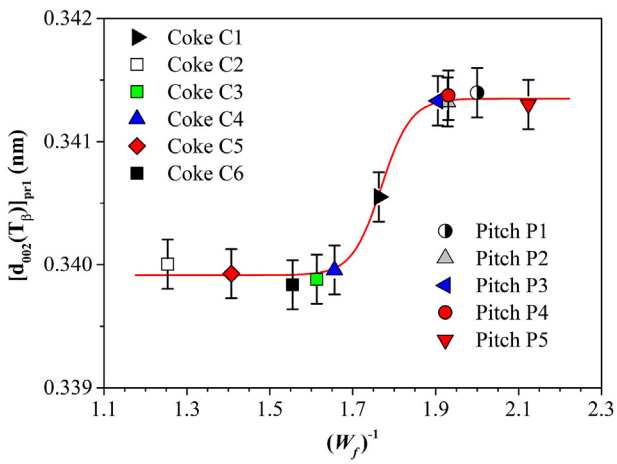

Fig. 15. Comparison between the experimental measurements of $d_{002}(T_\beta)$ of Tables 3 and 4 and the results of Eq. (32) (where $S_1 = 0.0014$ nm, $B_1 = 50$, $d_{002}(T_\beta)_{min} = 0.3399$ nm, $W_c = 0.57$) as a function of W_f ($0.45 < W_f < 0.85$) for the misorientation class G7(pr_1). The operating parameters of the heat treatment process to obtain this data (pr_1 process) are $HR_1 \sim 4\ ^\circ Cmin^{-1}$ and $t_{hold,1} = 10$ min. T_β was arbitrarily defined as 2400 K in Section 2.3. The experimental error [65] on $d_{002}(T_\beta)$ measurements is, at best, 2×10^{-4} nm. (A colour version of this figure can be viewed online.)

Combining Equations (30) and (31) yields:

$$\left[d_{002}\left(T_\beta\right) - d_{002}\left(T_\beta\right)_{min}\right]_{pr_1} = \frac{S_1}{1 + e^{-B_1\left(\frac{W_c}{W_F} - 1\right)}} \quad ; \text{ for } 0.45 < W_f < 0.85 \tag{32}$$

To validate the present development of Eq. (25) (i.e Eq. (32)), Fig. 15 presents the relevant results in the $0.45 < W_f < 0.85$ region for the present class of carbons (class G7(pr_1)). From Fig. 15, it is concluded that Eq. (32) is in good agreement (NS > 0.99) with the experimental data of the selected graphitizable carbons. However, it is premature to state that the present reasoning could readily apply to other classes of carbons. Additional graphitization data is needed as to avoid speculative conclusions on the effect of a change of misorientation class (through either a decrease or increase in L^{LMO}) on the parameters of Fig. 15 (e.g. S_1, $d_{002}(T_\beta)_{min}$, W_c). This endeavour is beyond the scope of the present paper. The aim here is only to show that it is possible to develop Eq. (25) for single class of graphitizable carbons with Eq. (32). Nonetheless, considering the excellent agreement presented in Fig. 15, it is reasonable to conclude that Eq. (32) is an acceptable *limited* development of Eq. (25) under the restrictions that a given carbon belongs to the misorientation class G7(pr_1).

Table 5

Measured values of the oxygen/hydrogen ratios $\left(\frac{\%O_{at.}}{\%H_{at.}}\right)$ and associated graphitization resistances (Ψ) of various green petroleum cokes (C1, C2, C3, C4, C5, C6) following heat treatment at $T_{semicoke}$ under pr_1 conditions. Values of $d_{002}(T_\alpha)$ are also presented for said carbons following heat treatment at T_α under pr_1 conditions. For all carbons, the sulfur weight content ($\%S_{wt.}$) following heat treatment at $T_{semicoke}$ is less than S_{low} ($\sim$ 9% wt.). Thus, Ψ can be calculated with Eq. (28). The value [5,19] of $T_{semicoke}$ in the present work is 823 K. T_α was arbitrarily defined at 2073 K in Section 2.3. The experimental error on the oxygen/hydrogen ratio is $\sim 2 \times 10^{-3}$. The experimental error on Ψ is $\sim 4 \times 10^{-3}$. The experimental error [65] on $d_{002}(T_\beta)$ measurements is, at best, 2×10^{-4} nm.

	C1	C2	C3	C4	C5	C6
Measured property						
$\%O_{at.}$ / $\%H_{at.}$	0.047	0.035	0.057	0.050	0.055	0.051
Ψ	0.083	0.044	0.092	0.082	0.078	0.080
$d_{002}(T_\alpha)$ (nm)	0.3432	0.3428	0.3425	0.3428	0.3427	0.3425
$\%S_{wt.}$	1.1	1.7	3.2	1.8	2.5	2.4

Table 6

Measured values of the oxygen/hydrogen ratios $\left(\frac{\%O_{at.}}{\%H_{at.}}\right)$ and associated graphitization resistances (Ψ) of various coal tar pitches (P1, P2, P3, P4, P5) following heat treatment at $T_{semicoke}$ under pr_1 conditions. Values of $d_{002}(T_\alpha)$ are also presented for said carbons following heat treatment at T_α under pr_1 conditions. For all carbons, the sulfur weight content ($\%S_{wt.}$) following heat treatment at $T_{semicoke}$ is less than S_{low} ($\sim$ 9% wt.). Thus, Ψ can be calculated with Eq. (28). The value [5,19] of $T_{semicoke}$ in the present work is 823 K. T_α was arbitrarily defined at 2073 K in Section 2.3. The experimental error on the oxygen/hydrogen ratio is $\sim 2 \times 10^{-3}$. The experimental error on Ψ is $\sim 4 \times 10^{-3}$. The experimental error [65] on $d_{002}(T_\beta)$ measurements is, at best, 2×10^{-4} nm.

	P1	P2	P3	P4	P5
Measured property					
$\%O_{at.}$ / $\%H_{at.}$	0.002	0.005	0.001	0.002	0.004
	0.003	0.009	0.003	0.003	0.008
$d_{002}(T_\alpha)$ (nm)	0.3431	0.3431	0.3431	0.3431	0.3431
	< 0.5	< 0.5	< 0.5	< 0.5	< 0.5

3.4. First-order non-homogeneous differential equation model for the calculation of δ_{002} as a function of ψ

Tables 5and 6 present the measured oxygen/hydrogen atomic ratios following heat treatment at $T_{semicoke}$. The $d_{002}(T_\alpha)$ values and Ψ values are also presented. For all carbons (C1, C2, C3, C4, C5, C6, P1, P2, P3, P4, P5), the measured sulfur content following heat treatment at $T_{semicoke}$ was found to be well below S_{low}. Hence, Eq. (28) calculates Ψ for the samples.

To model the data of Tables 5 and 6, a final *Ansatz* is required:

Ansatz 4: "Considering Ψ as some dimensionless force which resists graphitization, considering δ_r as a dimensionless displacement (δ_r independent of Ψ), the dimensionless work (W_{mf}) associated to the merging and flattening process between T_β and T_α (remembering that $T = T_{HT}$) is estimated with Eq. (33)."

$$W_{mf} \sim \Psi\ \delta_r \tag{33}$$

From Eq. (33), the following proportionality can be mathematically derived:

$$\frac{1}{\delta_r}\frac{d\delta_r}{d\Psi} \propto \frac{1}{\Psi} \tag{34}$$

The proportionality of Eq. (34) is the premise of the present development of Eq. (26) ($[\delta_{002}]_{pr_1} = f(W_f)$). The aim of said development is the accurate reproduction of the data of Tables 5 and 6 The following first-order non-homogeneous differential equation (Eq. (35)) is the selected approach to develop Eq. (26)

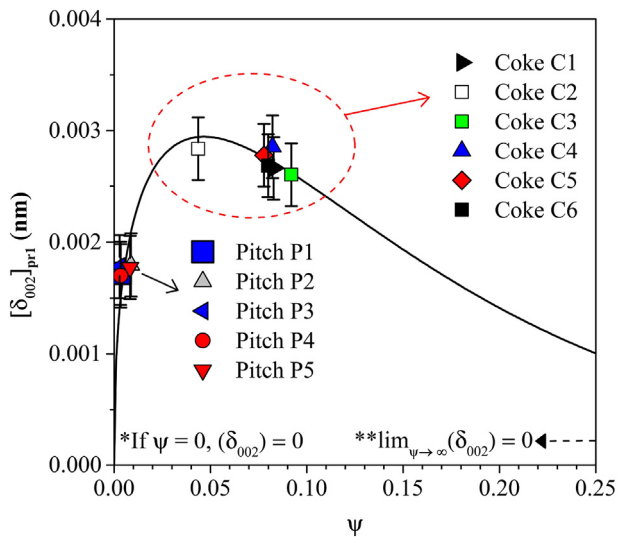

Fig. 16. Comparison between the experimental measurements of δ_{002} as a function of Ψ (Tables 5 and 6) and the results of Eq. (36) (where $C_2 = 12.5$, $a = 0.4$, $b = 8.6$). The operating parameters of the heat treatment process (process pr_1) to obtain the experimental data are $HR_1 \sim 4\ ^\circ Cmin^{-1}$ and $t_{hold,1} = 10$ min. The experimental error [65] on $d_{002}(T_\beta)$ measurements is, at best, 2×10^{-4} nm. (A colour version of this figure can be viewed online.)

which meets this aim while accounting for the proportionality of Eq. (34):

$$\frac{1}{\delta_r}\frac{d\delta_r}{d\Psi} = \frac{a}{\Psi} - b \tag{35}$$

In Eq. (35), a and b are fitting parameters which are adjusted to best reproduce the data. Integrating Eq. (35) yields:

$$\left[\frac{\delta_{002}}{\delta_c}\right]_{pr_1} = C_2\frac{\Psi^a}{e^{b\cdot\Psi}} \tag{36}$$

In Eq. (36), C_2 is the integration constant of Eq. (35). δ_c was previously defined in Table 2 (Section 2.4). Adequate fitting of the parameters of Eq. (36) provides a mathematical function which can reproduce the data of Tables 5 and 6 (data obtained under pr_1 conditions). The results are presented in Fig. 16.

It is concluded that Eq. (36) is in good agreement (NS = 0.83) with the experimental data obtained from the heat treatment of some graphitizable carbons. At the 0.05 level, Pearson, Spearman and Kendall correlation tests did not reveal significant correlation in our experimental data between W_f and Ψ. The range of application of Eq. (36) should be limited to $0 < \Psi < 0.1$ and to carbons heat treated under pr_1 conditions. To validate Eq. (36) at $\Psi > 0.1$ values, a greater variety of graphitizable and non-graphitizable carbons would need to be studied. However, this is beyond the scope of the present work.

Nonetheless, two theoretical aspects concerning the mathematical limits of Eq. (36) can be extracted from analysing Fig. 16. First, the case when Ψ is equal to 0. Physically, this represents a zero resistance LMO which is only possible if said LMO is composed of a single coke crystallite (i.e. $L_a = L^{LMO}$). This is explained by the fact that the graphitization resistance is a consequence of the densification of the IM during merging and flattening. Thus, if the LMO is composed of single crystallite, this difficulty is de facto null as no IM is present in the structure. Another feature concerns the limit of Eq. (36) as Ψ approaches infinity ($\lim_{\Psi\to\infty}(\delta_{002}) = 0$). This represents the case scenario where, for very small LMOs (a property correlated to high values of the oxygen/hydrogen ratio following primary carbonization), the merging and flattening process will not be able to reorganize the structure in a notable fashion. This is due to the intrinsic high generation of NADs relative to the generation and annealing of ATDs as small L^{LMO} values are associated to high surface/volume ratios for the LMOs (which favours the formation of NADs over ATDs). According to the present graphitization mechanism, these two theoretical limits must be respected regardless of the mathematical approach to Eq. (26). The fact that Eq. (36) respects those limits while simultaneously reproducing the available experimental data reinforces its validity in view of the present work.

Combining Eq. (36) with the mathematical development presented in Section 2.3 provides some additional theoretical understanding on the reorganisation behaviour during graphitization heat treatment of some atypical carbons (e.g. the high perfection non-graphitizable catalytically-produced graphenic carbons previously discussed [16]). Let us suppose that some high temperature process operating at $T \sim 2073$ K produces a hypothetical non-graphitic carbon (named PG-1) characterized by $d_{002} = X$ (where X is some arbitrary d_{002} value significantly greater than 0.3354 nm), $L_a = L^{LMO}$, a very high carbon content (almost all heteroatoms have been removed following heat treatment at 2073 K) and a ATD-free inner structure for the coke crystallites (where LMO is a single crystallite as $L_a = L^{LMO}$). As no IM is present in PG-1, the graphenic layers of the coke crystallite would remain of high perfection (relative to other carbons where $L_a \ll L^{LMO}$) as any densified IM distorts the LMO. The following question thus arises: would PG-1 graphitize following any given heat treatment process at $T > 2073$ K. Conceptually, as $L_a = L^{LMO}$, it can be implied that no IM would be present in PG-1. Hence, according to the present graphitization theory, the value of Ψ of PG-1 is null. Applying Eq. (36), this would imply a δ_{002} value of 0 (independent of the heat treatment process parameters). Combining this information with Equations (7), (8) and (18) results in the following equality (Eq. (37)):

$$d_{002}(T = 2073\,\mathrm{K}) = d_{002}\left(T_\beta\right) = d_{002}(T_c) = d_{002}\left(T_e^0\right) = X \ ;\ \text{if } L_a = L^{LMO} \tag{37}$$

Consequently, as $L_a = L^{LMO}$, PG-1 will not graphitize following graphitization heat treatment. Indeed, to fuel the process, PG-1 would only have access to the consumption of NADs as a possible driving vector for the transformation of the structure. However, NADs have, by definition, a very high activation energy for their annealing process (which explains why they persist under normal heat treatment conditions). Hence, some IM (which transforms into ATDs during merging and flattening) is needed to drive the graphitization heat treatment process, a conclusion independent of the value of L^{LMO}. Therefore, it can be said that high L^{LMO} ATD-free non-graphitic carbons characterized by $L^{LMO} = L_a$ are non-graphitizable. In contrast, high L^{LMO} non-graphitic carbons characterized by $L^{LMO} > L_a$ can potentially graphitize (to some extent) as they contain some amount of IM in their intra-LMO structure (as ATDs form from the temperature-densified IM).

4. Conclusion

The present paper discussed the groundwork of a new theory for the graphitization heat treatment process. It is inspired from the work of Ouzilleau [7], Franklin [1], Oberlin [5] and Harris [3]. This theory provides a better understanding of graphitizability by representing the graphitization heat treatment process as a topological mechanism (Fig. 3). This topology-based model successfully

reproduced the graphitization function ($d_{002}(T)$) of various non-graphitizable and graphitizable carbons. According to the developed approach, all carbons (non-graphitizable and graphitizable) "graphitize" to some extent. This claim is based on one of the key statements of the Oberlin model which is that all carbons are built, for the most part, of graphitizable units of variable graphitizability (i.e. the LMOs of Oberlin). Said units possess a finite graphitization potential at 3400 K (i.e. the Ultimate Graphitizability). Only LMOs may graphitize in non-graphitizable and graphitizable carbons following graphitization heat treatment. According to the present theory, the graphitizability of a carbon is generally proportional to the extent (L^{LMO}) of its constituting LMOs. High L^{LMO} values generally result in better graphitizability and small L^{LMO} values in poor graphitizability. Thus, non-graphitizable carbons, which poorly graphitize, mostly contain small LMOs. The key distinction of this theory is its ability to predict graphitizability as a continuous spectrum ranging from graphitizable to non-graphitizable carbons. Future work will explore the theory for a wider variety of more exotic graphitizable and non-graphitizable carbons in order to better understand the fundamental nature of graphitizability and the limits of thermodynamic descriptors for graphitization.

Acknowledgements

The authors are thankful to Professor Malcolm Heggie for valuable discussions. We would also like to thank Dr Martin Brassard for his support regarding the design of the carbonization and graphitization experiments. This project was supported by the Natural Sciences and Engineering Research Council of Canada, Alcoa, Hydro Aluminium, Constellium, Rio Tinto and the FRQNT.

References

[1] R.E. Franklin, Crystallite growth in graphitizing and non-graphitizing carbons, Proc. Roy. Soc. Lond. 209 (1951a) 196–218.
[2] R.E. Franklin, The structure of graphitic carbons, Acta Crystallogr. 4 (1951b) 253–261.
[3] P. Harris, New perspectives on the structure of graphitic carbons, Crit. Rev. Solid State Mater. Sci. 30 (2005) 235–253.
[4] D.B. Fischbach, The kinetics and mechanism of graphitization, in: Chemistry and Physics of Carbon, vol. 7, Marcel Dekker, 1971, pp. 1–97.
[5] A. Oberlin, Carbonization and graphitization, Carbon 22 (1984) 521–541.
[6] P. Harris, S. Tsang, High-resolution electron microscopy studies of non-graphitizing carbons, Philos. Mag. A 76 (1997) 667–677.
[7] P. Ouzilleau, A.E. Gheribi, P. Chartrand, Thermodynamic description of graphitizable carbons and the irreversible graphitization process, Carbon 132 (2018) 556–564.
[8] D. van Krevelen, Coal, third ed., Elsevier, 1993.
[9] A. Oberlin, S. Bonnamy, K. Oshida, Landmarks for graphitization, Tanso 224 (2006) 281–298.
[10] M. Villey, A. Oberlin, A. Combaz, Influence of elemental composition on carbonization pyrolysis of sporopollenin and lignite as models of kerogens, Carbon 17 (1979) 77–86.
[11] M. Monthioux, M. Oberlin, A. Oberlin, X. Bourrat, Heavy petroleum products: microtexture and ability to graphitize, Carbon 20 (1982) 167–176.
[12] J. Rouzaud, A. Oberlin, Structure, microtexture and optical properties of anthracene and saccharose-based carbons, Carbon 27 (1989) 517–529.
[13] X. Bourrat, A. Oberlin, J. Escalier, Microtextutre and structure of semi-cokes and cokes, Fuel 65 (1986) 1490–1500.
[14] S. Bonnamy, Carbonization of various precursors. effect of heating rate part ii: transmission electron microscopy and physicochemical studies, Carbon 37 (1999) 1707–1724.
[15] R. Vander Wal, A. Tomasek, K. Street, D. Hull, W. Thompson, Carbon nanostructure examined by lattice fringe analysis of high-resolution transmission electron microscopy images, Appl. Spectrosc. 58 (2004) 230–237.
[16] M. Monthioux, Structure, texture and thermal behaviour of polyaromatic solids, in: Carbon Molecules and Materials, Taylor and Francis, 2002, pp. 127–177.
[17] A. Oberlin, High-resolution TEM studies of carbonization and graphitization, in: Chemistry and Physics of Carbon, vol. 22, Marcel Dekker, 1989, 1–143.
[18] A. Oberlin, S. Bonnamy, P. Rouxhet, Colloidal and supramolecular aspects of carbon, in: Chemistry and Physics of Carbon, vol. 26, Marcel Dekker, 1999, 1–148.
[19] P. Ouzilleau, A.E. Gheribi, P. Chartrand, The graphitization temperature threshold analyzed through a second-order structural transformation, Carbon 109 (2016a) 896–908.
[20] J. Eck, J.L. Sans, M. Balat-Pichelin, Experimental study of carbon materials behavior under high temperature and VUV radiation; Application to Solar Probe+ heat shield, Appl. Surf. Sci. 257 (2011) 3196–3204.
[21] K. Zaghib, M. Dontigny, A. Guerfi, P. Charest, I. Rodrigues, A. Mauger, C. Julien, Safe and fast-charging Li-ion battery with long shelf life for power applications, J. Power Sources 196 (2011) 3949–3954.
[22] H. Coromina, D. Walsh, R. Mokaya, Biomass-derived activated carbon with simulatenously enhanced CO2 uptake for both pre and post combustion capture applications, J. Mater. Chem. 4 (2016) 280–289.
[23] P. Ouzilleau, A.E. Gheribi, G. Eriksson, D.K. Lindberg, P. Chartrand, A size-dependant thermodynamic model for coke crystallites: the carbon-hydrogen system up to 2500 K, Carbon 85 (2015) 99–118.
[24] E. Fitzer, K. K.-H, H. Boehm, H. Marsh, Recommended terminology for the description of carbon as a solid, Pure Appl. Chem. 67 (1995) 473–506.
[25] L. Ban, D. Crawford, H. Marsh, Lattice resolution electron microscopy in structural studies of non-graphitizing carbons from polyvinylidene chloride (PVDC), J. Appl. Crystallogr. 8 (1975) 415–420.
[26] J. Diaz, G. Paolicelli, S. Ferrer, F. Comin, Separation of the sp3 and sp2 components in the C1s photoemission spectra of amorphous carbon films, Phys. Rev. B 54 (1996) 8064–8069.
[27] A. Oberlin, S. Bonnamy, A realistic approach to disordered carbons, in: Chemistry and Physics of Carbon, vol. 31, Marcel Dekker, 2013, pp. 1–84.
[28] H. Terrones, A. Mackay, The geometry of hypothetical curved graphite structures, Carbon 30 (1992) 1251–1260.
[29] A. Botan, F. Ulm, R. Pellenq, B. Coasne, Bottom-up model of absorption and transport in multiscale porous media, Phys. Rev. 91 (2015), 0321331–10.
[30] A. Pelton, Phase Diagrams and Thermodynamic Modeling of Solutions, Elsevier, 2018.
[31] G. Lebon, D. Jou, J. Casas-Vazquez, Understanding Non-equilibrium Thermodynamics, Springer, 2008.
[32] S. Swegle, Irreversible phase transitions and wave propagation in silicate geologic materials, J. Appl. Phys. 68 (1990) 1563–1579.
[33] G. Duvall, R. Graham, Phase transitions under shock-wave loading, Rev. Mod. Phys. 49 (1977) 523–579.
[34] Q. Wu, F. Jing, Thermodynamic equation of state and application to hugoniot predictions for porous materials, J. Appl. Phys. 80 (1996) 4343–4349.
[35] M. Monthioux, J.C. Charlier, Giving credit where credit is due: the Stone(-Thrower) Wales designation revisited, Carbon 75 (2014) 1–4.
[36] W. Wu, J. Yin, W. Xie, W. Zhang, B. Wu, Y. Jiang, P. Zhang, Y. Ding, Effect of vacancy distribution on the relaxation properties of graphene: a molecular dynamics study, Micro & Nano Lett. 10 (2015) 693–695.
[37] W. Tian, W. Li, W. Yu, X. Liu, A review on lattice defects in graphene: types, generation, effects and regulation, Micromachines 8 (2017) 163.
[38] B. Jeong, J. Ihm, W. Yu, G. Lee, Stability of dislocation defect with two pentagon-heptagon pairs in graphene, Phys. Rev. B 78 (2008) 165403.
[39] O. Yazyev, S. Louie, Topological defects in graphene: dislocations and grain boundaries, Phys. Rev. B 81 (2010) 195420.
[40] G. Dienes, Mechanism for self-diffusion in graphite, J. Appl. Phys. 23 (1952) 1194–1200.
[41] J. Ma, D. Alfe, A. Michaelides, E. Wang, Stone-wales defects in graphene and other planar sp2-bonded materials, Phys. Rev. B 80 (2009), 0334071–4.
[42] T. Hamada, M. Furuyama, Y. Sajiki, T. Tomioka, Structures and electric properties of pitch-based carbon fibers heat-treated at various temperatures, J. Mater. Res. 5 (1990) 570–577.
[43] S. Brandtzaeg, Structural Changes during Calcination of Coke and Anthracite, Ph.D. thesis, Norwegian Institute of Technology, 1985.
[44] F.V. Fair, F.M. Collins, Effect of residence time on graphitization at several temperatures, in: Fifth Carbon Conference, Pergamon Press, 1961, pp. 503–508.
[45] H. Fujimoto, The production method of mesocarbon microbeads and their application, Tanso 241 (2010) 10–14.
[46] Y. Hishiyama, Y. Kaburagi, Parametrical representation of graphitization degree and preferred orientation of graphitizing cokes by magnetoresistance, Tanso 98 (1979) 89–95.
[47] Y. Hishiyama, K. Igarashi, I. Kanaoka, H. Fujii, T. Kaneda, T. Koidesawa, Y. Shimazawa, A. Yoshida, Graphitization behavior of Kapton-derived carbon film related to structure, microstructure and transport properties, Carbon 35 (1997) 657–668.
[48] J. Jimenez Mateos, E. Romero, C. Gomez de Salazar, XRD study of petroleum cokes by line profile analysis: relations among heat treatment, structure, and sulphur content, Carbon 31 (1993) 1159–1178.
[49] C. Kim, T. Fujino, K. Miyashita, T. Hayashi, M. Endo, M. Dresselhaus, Microstructure and electrochemical properties of boron-doped mesocarbon microbeads, J. Electrochem. Soc. 147 (2000) 1257–1264.
[50] J. Okada, A. Sekiguchi, T. Ishii, Effect of rapid heat treatment on the properties of carbon, in: Fifth Carbon Conference, Pergamon Press, 1961, pp. 497–502.
[51] J. Goma, Évolution thermique d'une couche mince de carbone: Variation du potentiel de sortie et structure cristalline, Ph.D. thesis, Université d'Orléan, 1978.
[52] I. Rannou, V. Bayot, M. Lelaurain, Structural characterization of graphitization process in pyrocarbons, Carbon 32 (1994) 833–843.
[53] B. Vazquez-Santos, E. Geissler, K. Laszlo, J.-N. R, A. Martinez-Alonso, J. Tascon, Graphitization of highly porous carbons derived from poly(p-phenylene benzobisoxazole), Carbon 50 (2012a) 2929–2940.

[54] B. Vazquez-Santos, E. Geissler, K. Laszlo, J.N. Rouzaud, A. Martinez-Alonso, J. Tascon, Comparative XRD, Raman, and TEM study on graphitization of PBO-derived carbon fibers, J. Phys. Chem. C 116 (2012b) 257–268.
[55] H. Cheng, H. Endo, T. Okabe, K. Saito, G. Zheng, Graphitization behaviour of wood ceramics and bamboo ceramics as determined by X-Ray diffraction, J. Porous Mater. 6 (1999) 233–237.
[56] M. Okada, M. Tatsumi, N. Ohta, Kinetic studies on the changes in structural and physical properties of isotropic graphite during graphitization, Tanso 252 (2012) 54–62.
[57] J. Maire, Recherche sur le phénomène de la graphitization, Ph.D. thesis, Thèse d'État Paris Schiffer, 1967.
[58] E. Heintz, Crystallite growth and ordering of cokes in the pre-graphitization temperature range, in: Proceedings of the Fifth London International Carbon and Graphite Conference, 1978, pp. 575–587.
[59] S. Yamada, H. Sato, T. Ishii, Eigenschaften und verwendung von glasartigem kohlenstoff, Carbon 2 (1964) 253–260.
[60] D. Fischbach, Magnetic suceptibility of glassy carbon, Carbon 5 (1967) 565–570.
[61] C. Kim, K. Yang, Heat treatment temperature effect on structural and chemical properties of pvdc-based disordered carbons, J. Mater. Sci. 38 (2003) 2987–2991.
[62] K. Kobayashi, S. Sugawara, S. Toyoda, H. Honda, An X-Ray diffraction study of phenol-formaldehyde resin carbons, Carbon 6 (1968) 359–363.
[63] L. Pesin, E. Baitinger, A new structural model of glass-like carbons, Carbon 40 (2002) 295–306.
[64] F. Rousseaux, D. Tchoubar, Structural evolution of a glassy carbon as a result of thermal treatment between 1000 et 2700 C - II, Carbon 15 (1977) 63–68.
[65] N. Iwashita, C. Park, H. Fujimoto, M. Shiraishi, M. Inagaki, Specification for a standard procedure of x-ray diffraction measurements on carbon materials, Carbon 4 (2004a) 701–714.
[66] P. Ouzilleau, A.E. Gheribi, D.K. Lindberg, P. Chartrand, A size-dependent thermodynamic model for coke crystallites: the carbon-sulfur system up to 2500 K, Metall. Mater. Trans. B 47B (2016b) 1817–1831.
[67] J. Nash, J. Sutcliffe, River flow forecasting through conceptual models part I : a discussion of principles, J. Hydrol. 10 (1970) 282–290.
[68] F. Grondvold, Heat capacities in critical regions, Pure Appl. Chem. 47 (1976) 251–266.
[69] J. Abrahamson, The surface energies of graphite, Carbon 11 (1973) 337–362.
[70] E. Fitzer, S. Weisenburge, Graphitization studies by in situ x-ray technique, Carbon 12 (1974) 657–666.
[71] P. Walker, H. McKinstry, J. Pustinger, X-Ray diffraction studies on carbon gasification, Ind. Eng. Chem. 46 (1954) 1651–1658.
[72] T. Peters, R. Jenkins, A. Scaroni, P. Walker, The importance of carbonization conditions on the character of phenanthrene coke and its graphitizability, Carbon 29 (1991) 981–990.
[73] X. Bourrat, A. Oberlin, J. Escalier, Sulphur behaviour during asphalt heat-treatment, Fuel 66 (1987) 542–550.
[74] J. Kipling, P. Shooter, R. Young, The effect of sulphur on the graphitization of carbons derived from polyvinyl chloride-sulphur systems, Carbon 4 (1966) 333–338.
[75] N. Iwashita, C. Park, H. Fujimoto, M. Shiraishi, M. Inagaki, Corrigendum to specification for a standard procedure of x-ray diffraction measurements on carbon materials [Carbon 42 (2004)701714], Carbon 42 (2004b) 2131.